

# Predicting the properties of binary stellar systems: the evolution of accreting protobinary systems

Matthew R. Bate<sup>1,2\*</sup>

<sup>1</sup> *Institute of Astronomy, Madingley Road, Cambridge CB3 0HA*

<sup>2</sup> *Max-Planck-Institut für Astronomie, Königstuhl 17, D-69117 Heidelberg, Germany*

Accepted 1999 December 23. Received in original form 1999 September 16

## ABSTRACT

We investigate the formation of binary stellar systems. We consider a model where a ‘seed’ protobinary system forms, via fragmentation, within a collapsing molecular cloud core and evolves to its final mass by accreting material from an infalling gaseous envelope. This accretion alters the mass ratio and orbit of the binary, and is largely responsible for forming the circumstellar and/or circumbinary discs.

Given this model for binary formation, we predict the properties of binary systems and how they depend on the initial conditions within the molecular cloud core. We predict that there should be a continuous trend such that closer binaries are more likely to have equal mass components and are more likely to have circumbinary discs than wider systems. Comparing our results to observations, we find that the observed mass-ratio distributions of binaries and the frequency of circumbinary discs as a function of separation are most easily reproduced if the progenitor molecular cloud cores have radial density profiles between uniform and  $1/r$  (e.g. Gaussian) with near uniform-rotation. This is in good agreement with the observed properties of pre-stellar cores. Conversely, we find that the observed properties of binaries cannot be reproduced if the cloud cores are in solid-body rotation and have initial density profiles which are strongly centrally condensed. Finally, in agreement with the radial-velocity searches for extra-solar planets, we find that it is very difficult to form a brown dwarf companion to a solar-type star with a separation  $\lesssim 10$  AU, but that the frequency of brown dwarf companions should increase with larger separations or lower mass primaries.

**Key words:** accretion, accretion discs – brown dwarfs – binaries: general – circumstellar matter – stars: formation – stars: mass function

## 1 INTRODUCTION

The favoured mechanism for producing most binary stellar systems is the fragmentation of a molecular cloud core during its gravitational collapse. Fragmentation can be divided into two main classes: direct fragmentation (e.g. Boss & Bodenheimer 1979; Boss 1986; Bonnell et al. 1991, 1992; Bonnell & Bastien 1992; Nelson & Papaloizou 1993; Burkert & Bodenheimer 1993; Bate & Burkert 1997), and rotational fragmentation (e.g. Norman & Wilson 1978; Bonnell 1994; Bonnell & Bate 1994a, 1994b; Burkert & Bodenheimer 1996; Burkert, Bate, Bodenheimer 1997). Direct fragmentation depends critically on the initial density structure within the molecular cloud core (e.g. non-spherical shape or density perturbations), whereas rotational fragmentation is relatively independent of the initial density structure of the

cloud because the fragmentation occurs due to nonaxisymmetric instabilities in a massive rotationally-supported disc or ring.

The main conclusion, from  $\approx 20$  years of fragmentation studies, is that it appears to be possible to form binaries with similar properties to those that are observed. However, it has not been possible to use these calculations to predict the fundamental properties of stellar systems such as the fraction of stellar systems which are binary or the properties of binary systems (e.g. the distributions of mass ratios, separations, and eccentricities and the properties of discs in pre-main-sequence systems).

There are two primary reasons for this lack of predictive power. First, the results of fragmentation calculations depend sensitively on the initial conditions, which are poorly constrained. The second problem is that of accretion. In fragmentation calculations, the binary or multiple protostellar systems that are formed initially contain only a small frac-

\* E-mail: mbate@ast.cam.ac.uk

tion of the total mass of the original cloud (e.g. Boss 1986; Bonnell & Bate 1994b) with the magnitude of this fraction decreasing with the binary’s initial separation (see Section 6.1). To obtain the final parameters of a stellar system, a calculation must be followed until all of the original cloud material has been accumulated by one of the protostars or their discs. Unfortunately, due to the enormous range in densities and dynamical time-scales in such a calculation, this is very difficult. Thus far, only one calculation has followed the three-dimensional collapse of a molecular cloud core until  $> 90\%$  of the initial cloud was contained in the protostars or circumstellar/circumbinary discs (Bate, Bonnell & Price 1995). Because such calculations are so difficult to perform, it is impossible to perform the number of calculations that would be required to predict the statistical properties of binary stellar systems – even if we knew the distribution of initial conditions. On the other hand, if we can overcome this second difficulty, we can use observations of binary systems to better constrain the initial conditions for star formation.

Bate & Bonnell (1997) quantified how the properties of a binary system are affected by the accretion of a small amount of gas from an infalling gaseous envelope. They found that the effects depend primarily on the specific angular momentum of the gas and the binary’s mass ratio (see also Artymowicz 1983; Bate 1997). Generally, accretion of gas with low specific angular momentum decreases the mass ratio and separation of the binary, while accretion of gas with high specific angular momentum increases the separation, drives the mass ratio toward unity, and can form a circumbinary disc. From these results, they predicted that closer binaries should have mass ratios that are biased toward equal masses compared to wider systems.

In this paper, we use the results of Bate & Bonnell (1997) to develop a protobinary evolution code that enables us to follow the evolution of a protobinary system as it accretes from its initial to its final mass, but does so in far less time than would be required for a full hydrodynamic calculation. Using this code, we consider the following model for the formation of binary stellar systems. We assume that a ‘seed’ binary system is formed at the centre of a collapsing molecular cloud core, presumably via some sort of fragmentation. The protobinary system initial consists of only a small fraction of the total mass of the core. Subsequently, it accretes the remainder of the initial cloud (which is falling on to the binary) and its properties evolve due to the accretion. We consider the formation process to be complete when all of the original cloud’s material is contained either in one of the two stars or their surrounding discs. Our goal is to obtain predictions about the properties of binary stars that can be tested observationally, and to determine how these properties depend on the initial conditions (e.g. the density and angular momentum profiles) in the progenitor molecular cloud cores so that the initial conditions can be better constrained.

In Section 2, we describe the methods used to follow the evolution of accreting protobinary systems, and we present the results of various test calculations in Section 3. In Sections 4 and 5, we present results from calculations with a range of initial conditions which follow the evolution of accreting protobinary systems. From these results, in Section 6, we make predictions regarding the properties of binary

systems and compare them with the latest observations. These predictions are briefly summarised in Section 7.

Those readers more interested in our predictions of the properties of binary stars, rather than the method by which these predictions have been obtained, may care to move directly to Section 4.

## 2 COMPUTATIONAL METHODS

### 2.1 Protobinary evolution code

Bate & Bonnell (1997) considered the effects that accretion of a small amount of gas from an infalling gaseous envelope has on the properties of a protobinary system. They quantified these effects as functions of the mass ratio of the protobinary and the specific angular momentum of the infalling gas. Therefore, if a ‘seed’ binary system is formed at the centre of a collapsing gas cloud, and we know its initial mass ratio and separation, the mass infall rate on to the binary, and the distribution of the specific angular momentum of the gas, then we can determine how the binary will evolve as it accretes infalling gas. Essentially, we can integrate the binary from its initial mass to its final mass by accreting the gas in a series of small steps and altering the masses of the binary’s components and their orbit by the amounts determined by Bate & Bonnell (1997) after each step.

We now describe the implementation of the protobinary evolution (PBE) code. We begin with the properties of the molecular cloud core, before it begins to collapse dynamically, from which the binary system will form. For simplicity, the progenitor cloud (see Figure 1) is assumed to be spherical with mass  $M_c$ , radius  $R_c$ , density distribution

$$\rho = \rho_0 (r/R_c)^\lambda, \quad (1)$$

and angular velocity

$$\Omega_c = \Omega_0 (r/R_c)^\beta, \quad (2)$$

where  $\lambda$  controls the initial central condensation of the cloud, and  $\beta$  gives the amount of differential rotation of the cloud. Note that  $\Omega_c$  is constant on spheres ( $r$ ), not cylinders ( $r_{xy}$ ). Note also that if molecular cloud cores spend a large fraction of their lifetimes as magnetically-supported, quasistatic structures before undergoing dynamic collapse, they are likely to be in solid-body rotation and significantly centrally-condensed before the dynamic collapse begins.

We assume that a ‘seed’ binary is formed at the centre of this molecular cloud core after it begins to collapse. The ‘seed’ binary contains only a small fraction of the total mass of the cloud. The masses of the primary and secondary are  $M_1$  and  $M_2$ , respectively. The binary has a total mass  $M_b$ , mass ratio  $q = M_2/M_1$ , separation  $a$  and is in a circular orbit. We assume the binary has a circular orbit and that its axis of rotation is aligned with that of the cloud, since the PBE code makes use of the results of Bate & Bonnell (1997) and they only studied such systems.

The ‘seed’ binary is assumed to have formed from the gas that was in a spherical region at the centre of the progenitor cloud of radius  $R_b$  (Figure 1). Unless otherwise stated, we assume that this spherical region initially had the same mass and angular momentum as the ‘seed’ binary. Thus, the initial angular momentum of the binary is given by

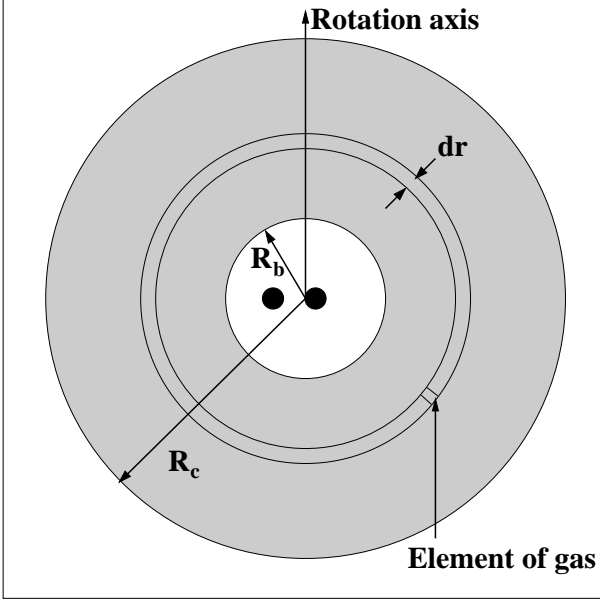


**Figure 1.** The model for binary star formation which is considered in this paper (see Section 2.1).

$$L_b = \sqrt{GM_b^3 a} \frac{q}{(1+q)^2} = \Lambda M_b R_b^2 \Omega_{Rb} = L_{cen} \quad (3)$$

where  $\Omega_{Rb} = \Omega_0 (R_b/R_c)^\beta$  and, for various values of  $\beta$  and  $\lambda$ ,

$$\Lambda = \frac{2(3+\lambda)}{3(5+\lambda+\beta)}. \quad (4)$$

For example, for an initially uniform-density cloud in solid-body rotation,  $\Lambda = 2/5$ . As in Bate & Bonnell (1997), we use natural units of  $M_b = 1$  and  $a = 1$  for the ‘seed’ binary, with  $G = 1$ .

In general, to evolve the binary under the accretion of gas from the remainder of the collapsing cloud, we would need to know the infall rate and the specific angular momentum distribution of the gas as functions of time (i.e. we would need to calculate how the cloud evolves as it collapses on to the binary). However, if we make two simple assumptions, we can calculate the evolution of the binary knowing only the density and angular momentum distributions of the cloud *before* it began to collapse. Furthermore, we can consider the evolution of the binary as a function of the mass that has been accreted from the envelope  $M_{acc}$ , and do not need to keep track of time explicitly. First, we assume that the specific angular momentum of each element of gas in the cloud is conserved during its fall until it gets very close to the binary. Second, we assume that the time it takes for gas to fall on to the binary from a radius  $r$  from centre of the cloud is independent of direction (i.e. the gas falls on to the binary in spherical shells).

These are reasonable assumptions if the molecular cloud core undergoes a dynamic collapse (i.e. the magnitude of its gravitational energy dominates the thermal, rotational and magnetic energies of the cloud). In principle, angular momentum transport between elements of gas could occur during collapse if the cloud has density inhomogeneities (via gravitational torques) or is threaded by magnetic fields (via

magnetic torques). However, if the collapse is dynamic, these effects are unlikely to have enough time to transport a significant amount of angular momentum, and even cores which are initially magnetically sub-critical typically evolve into configurations which undergo a dynamic collapse (e.g. Basu 1997).

The integration of the binary from its initial mass,  $M_{acc} = M_b = 1$ , to its final mass  $M_{acc} = M_c \geq M_b$  (since some of the gas could be contained in a circumbinary disc) under the accretion of the gas with  $r > R_b$  proceeds as follows (Figure 1). A spherical shell of gas with inner radius  $r = R_b$  and thickness  $\Delta r$  is divided into many elements such that the gas in each element has the same specific angular momentum (i.e. each ‘element’ consists of two rings of gas, one above and one below the orbital plane). The effect of each element of gas on the binary, when it is accreted, is determined using the results of Bate & Bonnell (1997) from its specific angular momentum, its mass, and  $q$  (see below). The effects on the binary from all the gas elements making up a shell are added together, and then the binary’s properties ( $M_b$ ,  $q$ ,  $a$ ) are updated. The mass of material that is not captured by one of the two protostars but that remains in a circumbinary disc (if any) is also determined. The process is repeated for the shell of material at radius  $r = R_b + \Delta r$  until the entire cloud of mass  $M_c$  has been exhausted.

The results from Bate & Bonnell (1997) are used to determine the effects on the binary of the accretion of an element of gas. The specific angular momentum of an element of gas relative to the specific angular momentum required for gas to form a circular orbit at a radius equal to the binary’s separation is given by

$$j_{rel} = \frac{r_{xy}^2 \Omega_c}{\sqrt{GM_b a}} \quad (5)$$

where  $r_{xy}$  is the cylindrical radius of the gas element from the axis of rotation in the progenitor cloud. To evolve the binary, we need to know the values of  $\dot{M}_1/\dot{M}_{acc}$ ,  $\dot{M}_2/\dot{M}_{acc}$  and  $(\dot{a}/a)/(\dot{M}_{acc}/M_b)$  as functions of  $j_{rel}$  and  $q$ , where  $\dot{M}_{acc}$  is the rate of accretion from the infalling envelope on to the binary. Note that we consider gas to be ‘accreted’ by one of the protostars if it is actually accreted onto the protostar itself or if it is captured in the protostar’s circumstellar disc (see also Section 3.2). These quantities were determined by Bate & Bonnell (1997) only at set intervals in  $q$ - $j_{rel}$ -space. Interpolation between these points is performed to determine the quantities for any given  $q$  and  $j_{rel}$ . Boundary conditions are used for  $q = 1$  and  $q = 0$ . For  $q = 1$ , we set  $\dot{M}_1/\dot{M}_{acc} = \dot{M}_2/\dot{M}_{acc}$  explicitly, with  $(\dot{a}/a)/(\dot{M}_{acc}/M_b)$  being determined from Bate & Bonnell (1997). For  $q = 0$ , we set  $\dot{M}_2/\dot{M}_{acc} = 0$  and

$$\dot{M}_1/\dot{M}_{acc} = \dot{M}_2/\dot{M}_{acc} = \begin{cases} 1 & \text{if } j_{rel} \leq 1, \\ 0 & \text{otherwise} \end{cases} \quad (6)$$

and  $(\dot{a}/a)/(\dot{M}_{acc}/M_b)$  is set equal to the values for  $q = 0.1$ . The evolution of a binary with an initial mass ratio  $q \gtrsim 0.05$  is insensitive to the assumptions for  $q = 0$ . This was tested by setting the primary and secondary accretion rates for  $q = 0$  equal to those for  $q = 0.1$  and repeating the calculations. Note that we use the values of  $(\dot{a}/a)/(\dot{M}_{acc}/M_b)$  that were derived by Bate & Bonnell (1997) for the effects of *accretion only*. We do not include any affect on the binary’s separation

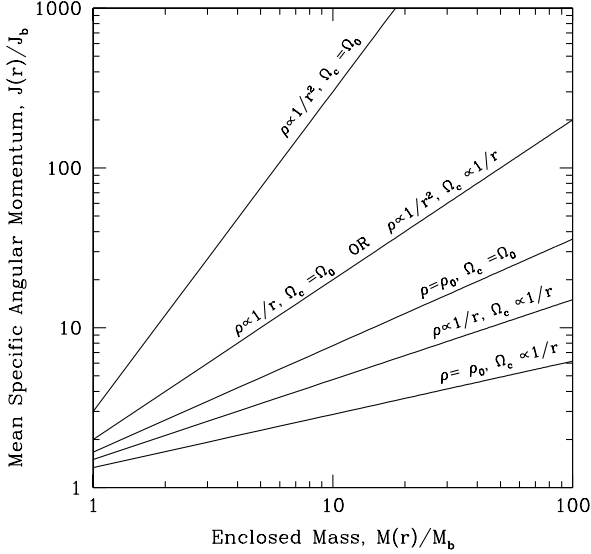


**Figure 2.** The relationship between angular momentum and mass for different types of molecular cloud core (equation 7). The values are normalised by the mean specific angular momentum and mass of the central region of gas from which the ‘seed’ binary forms (which are also equal to the mean specific orbital angular momentum and mass of the ‘seed’ binary itself). Notice that the angular momentum is greater initially and increases more rapidly with enclosed mass in clouds which are more centrally condensed or have less differential rotation ( $\beta \leq 0$ ). Also, the relation between angular momentum and mass is the same for a cloud with  $\rho \propto 1/r$  in solid-body rotation as it is for a cloud with  $\rho \propto 1/r^2$  and  $\Omega_c \propto 1/r$ .

due to the loss of orbital angular momentum to the gas in a circumbinary disc (if one exists).

From equation 3, we note that specifying the values of  $\Lambda$  and  $q$  fixes the relationship between the mean specific angular momentum of a *shell* of gas,  $J(r)$ , at radius  $r$ , and the enclosed mass,  $M(r)$ , in the progenitor cloud. For all  $q$ ,

$$\frac{J(r)}{J_b} = \frac{2}{3\Lambda} \left( \frac{M(r)}{M_b} \right)^{\left(\frac{2}{3\Lambda} - 1\right)} \quad (7)$$

where  $J_b = L_b/M_b$  is the mean specific angular momentum of the ‘seed’ binary, which depends on  $q$ . Equation 7 is plotted for various types of molecular cloud core in Figure 2. With progenitor cores that are more centrally-condensed, the specific angular momentum of the first gas to fall on to the ‘seed’ binary from the envelope is greater and increases more rapidly as mass is accreted than in less centrally-condensed cores. For cores which have a greater amount of differential rotation ( $\beta \leq 0$ ), the specific angular momentum of the gas is lower to begin with and increases more slowly as mass is accreted.

Since  $J_b$  in equation 7 depends on the mass ratio,  $q$ , and separation,  $a$ , of the ‘seed’ binary, the angular momentum of the cloud,  $J(r)$  is linked to the properties of the ‘seed’ binary (due to our use of equation 3). This can be viewed in two ways. First, if we consider a series of clouds with the same density and rotation profiles but that form ‘seed’ binaries with different mass ratios, then the separations of the

binaries will be somewhat larger for those with smaller mass ratios and  $J_b$  is the same for all mass ratios. Alternately, if we choose ‘seed’ binaries with the same separations, their progenitor clouds must be rotating more slowly for those binaries with lower mass ratios. We chose to use equation 3 because, for a ‘seed’ binary with a given mass ratio and separation, this gives the slowest possible rotation rate of the progenitor cloud. The progenitor cloud could be rotating more rapidly than this if some of the angular momentum of the gas from which the ‘seed’ binary formed is contained in circumstellar discs, but it could not be rotating more slowly.

Finally, since choosing  $\Lambda$  and  $q$  fixes the relationship between angular momentum and mass in the progenitor cloud (independent of  $M_c/M_b$ ,  $R_c$  and  $\Omega_0$ ), it follows that the evolution proceeds in the same way for any value of  $M_c/M_b$ . Thus, a graph which shows the *evolution* of a particular protobinary system as it accretes gas from its initial to its final mass can *also* be viewed as giving the *final states* of binaries that have accreted a certain amount of mass relative to their initial mass (e.g. Figures 9 to 14). This is only the case because we have chosen clouds that have scale-free density and angular momentum profiles, and does not apply, for example, to clouds with Gaussian density profiles that have a fixed inner to outer density contrast (e.g. 20:1).

## 2.2 Smoothed particle hydrodynamics code

To test the PBE code described above, we compare its results with those obtained from full hydrodynamic calculations using a three-dimensional, smoothed particle hydrodynamics (SPH) code. The SPH code is based on a version originally developed by Benz (Benz 1990; Benz et al. 1990). The smoothing lengths of particles are variable in time and space, subject to the constraint that the number of neighbours for each particle must remain approximately constant at  $N_{\text{neigh}} = 50$ . The SPH equations are integrated using a second-order Runge-Kutta-Fehlberg integrator with individual time steps for each particle (Bate et al. 1995). Gravitational forces between particles and a particle’s nearest neighbours are found by using either a binary tree, as in the original code, or the special-purpose GRAVITY-piPE (GRAPE) hardware. The implementation of SPH using the GRAPE closely follows that described by Steinmetz (1996). Using the GRAPE attached to a Sun workstation typically results in a factor of 5 improvement in speed over the workstation alone.

Calculations were performed using three different forms of artificial viscosity. The scatter in the results from calculations with different viscosities is used to give indication of the uncertainty in the SPH results. The viscosity,  $\Pi_{ij}$ , between particles  $i$  and  $j$  enters the momentum equation as

$$\frac{d\mathbf{v}_i}{dt} = - \sum_j m_j \left( \frac{P_i}{\rho_i^2} + \frac{P_j}{\rho_j^2} + \Pi_{ij} \right) \nabla_i W(r_{ij}, h_{ij}), \quad (8)$$

where  $\mathbf{v}$  is the velocity,  $t$  is the time,  $m$  is the particle’s mass,  $P$  is the pressure,  $\rho$  is the density,  $W$  is the SPH smoothing kernel,  $r_{ij}$  is the distance between particles  $i$  and  $j$ , and  $h_{ij}$  is the mean of the smoothing lengths of particles  $i$  and  $j$ . All formulations of the viscosity have linear and quadratic terms which are parameterised by  $\alpha_v$  and  $\beta_v$ , respectively. The first form of viscosity is the ‘standard’ form, originally

given by Monaghan & Gingold (1983) (see also Monaghan 1992)

$$\Pi_{ij} = \begin{cases} (-\alpha_v c_{ij} \mu_{ij} + \beta_v \mu_{ij}^2) / \rho_{ij} & \mathbf{v}_{ij} \cdot \mathbf{r}_{ij} \leq 0 \\ 0 & \mathbf{v}_{ij} \cdot \mathbf{r}_{ij} > 0 \end{cases} \quad (9)$$

where  $\rho_{ij} = (\rho_i + \rho_j)/2$ ,  $c_{ij} = (c_i + c_j)/2$  is the mean sound speed,  $\mathbf{v}_{ij} = \mathbf{v}_i - \mathbf{v}_j$ , and

$$\mu_{ij} = \frac{h_{ij} \mathbf{v}_{ij} \cdot \mathbf{r}_{ij}}{\mathbf{r}_{ij}^2 + 0.01 h_{ij}^2}. \quad (10)$$

This form is known to have a large shear viscosity. The second form (Monaghan & Gingold 1983; Hernquist & Katz 1989) has much less shear viscosity but does not reproduce shocks quite as well as the ‘standard’ formalism. It is given by

$$\Pi_{ij} = \frac{q_i}{\rho_i} + \frac{q_j}{\rho_j} \quad (11)$$

where

$$q_i = \begin{cases} \alpha_v h_i \rho_i c_i |\nabla \cdot \mathbf{v}|_i + \beta_v h_i^2 \rho_i |\nabla \cdot \mathbf{v}|_i^2 & (\nabla \cdot \mathbf{v})_i \leq 0 \\ 0 & (\nabla \cdot \mathbf{v})_i > 0 \end{cases} \quad (12)$$

The third form is that proposed by Balsara (1989) (see also Benz 1990), which is identical to the ‘standard’ form, except that  $\mu_{ij}$  is replaced by  $\mu_{ij}(f_i + f_j)/2$  where

$$f_i = \frac{|\nabla \cdot \mathbf{v}|_i}{|\nabla \cdot \mathbf{v}|_i + |\nabla \times \mathbf{v}|_i + \eta c_i / h_i} \quad (13)$$

and  $\eta = 1.0 \times 10^{-4}$ . In purely compressional flows this form gives the same results as that of the ‘standard’ viscosity, while in shearing flows the magnitude of the viscosity is reduced. The three forms of viscosity will be referred to as the Standard,  $\nabla \cdot \mathbf{v}$ , and Balsara forms, respectively.

Modelling of non-gaseous bodies (in this paper, the protostars), and the accretion of gas on to them, is achieved by the inclusion of sink particles (Bate et al. 1995; Bate 1995). These were also used by Bate & Bonnell (1997). A sink particle is a non-gaseous particle with a mass many times larger than that of an SPH gas particle. Any SPH gas particle that passes within a specified radius of the sink particle, the accretion radius  $r_{\text{acc}}$ , is accreted with its mass, linear momentum, and spin angular momentum being added to those of the sink particle. Sink particles interact with SPH gas particles only via gravitational forces. Boundary conditions can also be included for particles near the accretion radius (Bate et al. 1995), but they are not used for the calculations in this paper. Although boundary conditions are typically required to stop the erosion of discs near the accretion radius (Bate et al. 1995), this is not necessary here because once a disc forms it is replenished by the infalling gas more rapidly than it is eroded.

### 3 TESTING THE PROTOBINARY EVOLUTION CODE

To test how accurately the protobinary evolution (PBE) code (Section 2.1) describes the evolution of a ‘seed’ binary as it accretes from its initial to its final mass we performed several full SPH calculations for comparison. Two test cases were performed. The first follows the formation

of a binary system from the collapse of an initially uniform-density, spherical molecular cloud core in solid-body rotation. The ‘seed’ binary is assumed to have a mass ratio of  $q = 0.6$  and a mass of  $M_b = M_c/10 = 1$ . The second test case is similar, except that the progenitor cloud is centrally-condensed with a  $1/r$ -density distribution and there is less mass in the envelope relative to the initial binary’s mass:  $M_b = M_c/5 = 1$ .

#### 3.1 SPH initial conditions

##### 3.1.1 Test Case 1

The evolutions given by the PBE code are scale-free. However, for the SPH calculations, we choose to specify physical parameters. Test case 1 consists of the collapse of a uniform-density molecular cloud core in solid-body rotation with

$$\begin{aligned} M_c &= 1.0 M_\odot, & R_c &= 1.0 \times 10^{17} \text{ cm}, \\ T &= 10 \text{ K}, & \Omega_c &= 3.13 \times 10^{-14} \text{ rad s}^{-1}, \end{aligned} \quad (14)$$

where  $T$  is the temperature of the cloud, and it is assumed to consist of molecular hydrogen. The ‘seed’ binary is assumed to form from the mass initially contained within the sphere of radius  $R_b = 4.64 \times 10^{16}$  cm, which has  $1/10$  of the cloud’s total mass.

The initial conditions are evolved with  $2.0 \times 10^5$  SPH gas particles until the particles that were initially within  $R_b$  have collapsed to within  $r = 2 \times 10^{15}$  cm of the centre. At this point, the calculation is stopped and the particles that were contained within  $R_b$  are removed and replaced by a ‘seed’ binary system with the same mass as those particles that were removed ( $M_b = 0.1 M_\odot$ ). The binary has mass ratio  $q = 0.6$ , separation  $a = 1.0 \times 10^{15}$  cm and is in a circular orbit. Note that the rotation rate of the cloud,  $\Omega_c$ , is chosen so that the total angular momentum of the gas initially within  $R_b$  is equal to the orbital angular momentum of the ‘seed’ binary (the default used by the PBE code). The calculation is then restarted and the remaining gas begins to fall on to the binary. As the binary increases its mass by 5%, its mass ratio and separation are forced to evolve as predicted by the PBE code (to allow time for the gas to establish its correct flow pattern on to the binary). After this, however, the binary is free to evolve as the accretion of gas dictates.

##### 3.1.2 Test Case 2

The second test case consists of a  $1/r$ -density molecular cloud core in solid-body rotation with

$$\begin{aligned} M_c &= 1.0 M_\odot, & R_c &= 1.0 \times 10^{17} \text{ cm}, \\ T &= 10 \text{ K}, & \Omega_c &= 5.74 \times 10^{-14} \text{ rad s}^{-1}. \end{aligned} \quad (15)$$

The ‘seed’ binary is assumed to form from the mass initially contained within the sphere of radius  $R_b = 4.47 \times 10^{16}$  cm, which has  $1/5$  of the cloud’s total mass.

The initial conditions are evolved with  $1.0 \times 10^5$  SPH gas particles (half the number that were used for test case 1 due to the smaller mass of the cloud relative to the ‘seed’ binary) in an identical manner to test case 1.

### 3.2 Method

While the gas is modelled using SPH particles in the usual manner, the binary's components (the protostars) are modelled with sink particles (Section 2.2). Their accretion radii change in size as the mass ratio and separation of the binary changes and are always equal to  $r_{\text{acc}} = 0.1R_i$  where  $R_i$  are the sizes of the mean Roche lobes of the two protostars (Frank, King & Raine 1985)

$$R_1/a = 0.38 - 0.20 \log q, \quad 0.05 < q \leq 1, \quad (16)$$

for the primary and

$$R_2/a = \begin{cases} 0.38 + 0.20 \log q, & 0.5 \leq q < 1, \\ 0.462 (q/(1+q))^{1/3}, & 0 < q < 0.5, \end{cases} \quad (17)$$

for the secondary. This enables circumstellar discs of size  $\gtrsim 0.2R_i$  to be resolved by the SPH calculations. Smaller accretion radii would allow smaller discs to be resolved, but would also require more computational time due to the shorter dynamical time-scales.

As in Bate & Bonnell (1997), we define the mass of a protostar ( $M_1$  or  $M_2$ ) to be the mass of a sink particle and its *circumstellar disc* (if any). Hence, when stating the masses of the two components or mass ratio of the binary we are assuming that, in reality, all of the material in a circumstellar disc will eventually be accreted by its central star. Therefore, the binary's mass  $M_b$  is equal to the masses of the sink particles and their circumstellar discs. The parameters of the binary's orbit are calculated by considering these masses.

A gas particle belongs to a circumstellar disc if its orbit, calculated considering only one sink particle at a time, has eccentricity  $< 0.5$ , and semi-major axis  $< D/2$ . This simple criterion gives excellent extraction of the circumstellar discs. The mass of material in a circumbinary disc  $M_{\text{cb}}$  (if any), is defined as being the gas which has an outwards (positive) radial velocity or which is falling on to the binary more slowly than  $1/3$  of the local free-fall velocity (i.e.  $v_r > -1/3\sqrt{2GM_b/r}$ ) and which is not in one of the circumstellar discs as defined above or within distance  $a$  of the binary's centre of mass. The amount of gas that has fallen on to the binary from the envelope  $M_{\text{acc}}$  is defined as  $M_b + M_{\text{cb}}$  plus the remaining gas within  $a$  of the binary's centre of mass.

The equation of state of the gas is given by

$$P = K\rho^\gamma, \quad (18)$$

where  $P$  is the pressure,  $\rho$  is the density, and  $K$  is a constant that depends on the entropy of the gas. The ratio of specific heats  $\gamma$  varies with density as

$$\gamma = \begin{cases} 1.0, & \rho \leq 10^\eta \text{ g cm}^{-3}, \\ 1.4, & \rho > 10^\eta \text{ g cm}^{-3}. \end{cases} \quad (19)$$

The value of  $K$  is defined such that when the gas is isothermal  $K = c_s^2$ , with  $c_s = 2.0 \times 10^4 \text{ cm s}^{-1}$  for molecular hydrogen at 10 K. We choose  $\eta = -12$  for test case 1 and  $\eta = -13$  for test case 2. The heating of the gas at high densities inhibits fragmentation of the discs (e.g. Bonnell 1994; Bonnell & Bate 1994a; Burkert & Bodenheimer 1996; Burkert et al. 1997). In reality, this heating occurs when the gas becomes optically thick to infrared radiation. The results are independent of the exact density at which heating starts, so

long as the gas which falls on to the binary from the envelope is 'cold' (i.e. pressure forces are not dynamically important so that the gas falls freely on to the binary), the discs are relatively thin, and the discs do not fragment.

### 3.3 Test Case 1

The evolutions of test case 1 as given by the PBE and SPH codes are presented in Figure 3. We give the binary's mass ratio  $q$ , separation  $a$ , the ratio of the mass of the circumbinary disc (if one exists) to the mass of the binary  $M_{\text{cb}}/M_b$ , and the binary's eccentricity  $e$ , as functions of the mass which has been accreted from the cloud  $M_{\text{acc}}$  (up to 10 times the binary's initial mass). In addition, for two of the SPH calculations, we show snapshots at various times during the calculations (Figures 4 and 5).

#### 3.3.1 PBE calculation

The PBE code predicts that after the binary has accreted all the gas in the cloud, its mass ratio has increased from  $q = 0.6$  to  $q \approx 0.84$  while its separation, after decreasing initially, has returned to approximately the initial value. The binary's final mass is 8.8 times its initial mass with the remaining 12% of the cloud located in a circumbinary disc. With the PBE code, the binary is assumed to remain in a circular orbit throughout the evolution.

#### 3.3.2 SPH calculations

Three SPH calculations were performed using different formulations of the artificial viscosity: S1: Standard, with  $\alpha_v = 1$  and  $\beta_v = 2$ ; S2: Standard, with  $\alpha_v = 0.5$  and  $\beta_v = 2$ ; and B1: Balsara, with  $\alpha_v = 0.25$  and  $\beta_v = 1$ . S1 and S2 have the same formulation, but S2 has approximately half the shear viscosity that is present in S1 (the linear  $\alpha_v$ -viscosity dominates the shear viscosity in the code; the  $\beta_v$ -viscosity is only important in shocks). B1 has the lowest shear viscosity of the three, but also has a different formulation.

Unfortunately, the SPH calculations cannot be evolved until all of the original cloud has been accreted. The reason is that as the evolution proceeds, the rate at which mass falls on to the binary decreases and, thus, more orbits of the binary must be calculated for the same amount of mass to fall on to the binary. For example, the increase from  $M_b = 1$  to  $M_b = 2$  takes  $\approx 5$  orbits, while the increase from  $M_b = 4$  to  $M_b = 5$  takes  $\approx 14$  orbits. The CPU time required to evolve the binary until the entire cloud falls in is prohibitive, which, after all, is the reason that we developed the PBE code in the first place. It takes  $\approx 60$  orbits for the binary to increase its mass by a factor of 6 (i.e.  $\approx 60\%$  of the total cloud was accreted). Each of the three SPH calculations took 4–5 months on a 170 MHz Sun Ultra workstation with a GRAPE board. The evolution with the PBE code takes a few seconds!

#### 3.3.3 Evolution of the mass ratio and separation

Although the SPH calculations do not run to completion, we can compare the evolution as the binary's mass increases

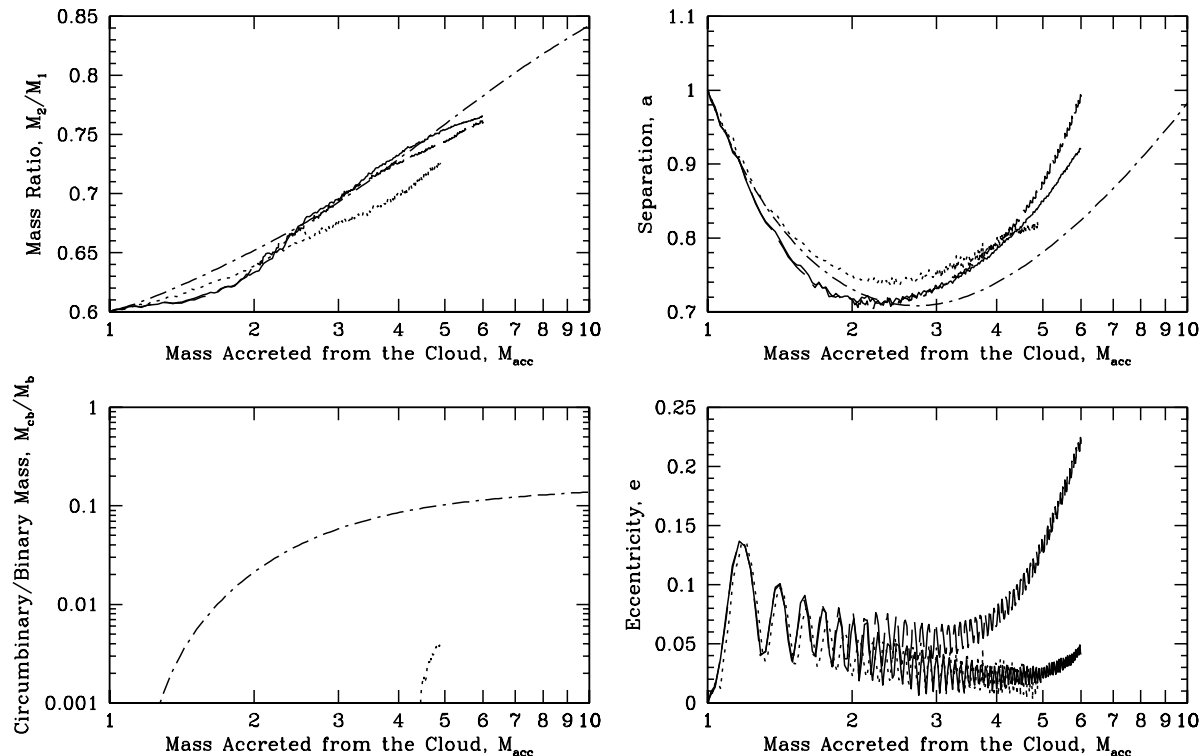


**Figure 3.** First comparison of the results from the protobinary evolution (PBE) code with those from the full SPH calculations. The graphs show the evolution of a protobinary system that was formed in the centre of a collapsing molecular cloud core which initially had a uniform density profile and was in solid-body rotation. The evolution of the (a; upper left) mass ratio, (b; upper right) separation, (c; lower left) ratio of mass in a circumbinary disc to that of the binary, and (d; lower right) eccentricity are plotted as the binary accretes gas from the infalling envelope. The dot-dashed lines show results from the PBE code. The other lines show the results from the full SPH calculations with artificial viscosities of S1 (long-dashed), S2 (solid), and B1 (dotted) (see Section 3.3.2).

by a factor of 5-6. Overall, there is excellent agreement between the PBE and SPH codes for the evolution of the mass ratio and separation. The mass ratio is predicted to within 5% over the entire evolution and the separation to within 20%. Indeed, there is as much scatter between the different SPH results as there is between the PBE results and the SPH results. Thus, **for the evolution of the mass ratio and separation, we conclude that the PBE code is at least as accurate as a full SPH calculation of this resolution.** Notice also that the PBE results (which assumed  $e = 0$ ) and SPH results are in good agreement even though the eccentricity varies between  $0 < e \lesssim 0.2$  during the SPH calculations. This implies that the evolution given by the PBE code is satisfactory, not just for circular binaries, but for binaries with  $e \lesssim 0.2$ .

### 3.3.4 Evolution of the circumbinary disc

The good agreement for the mass ratio and separation does not hold for the evolution of the circumbinary disc. The PBE code predicts that more gas will settle into a circumbinary disc than is found in the SPH calculations. Cases S1 and S2 do not form circumbinary discs at all for  $M_{\text{acc}} < 6$ , while B1 only begins to form a circumbinary disc when  $M_b \gtrsim 4.3$  (Figures 3c and 5). The difference between S1/S2 and B1 can be attributed to the much larger shear viscosity which is present in S1 and S2 compared to B1. Greater shear viscos-

ity inhibits the formation of a circumbinary disc by removing angular momentum from the gas which would otherwise settle into a circumbinary disc. Another problem is that, in all of the SPH calculations, the binary has a larger separation than is predicted by the PBE code when  $M_{\text{acc}} \gtrsim 2.3$  which also inhibits the formation of a circumbinary disc. These problems of circumbinary disc formation are the main reason that we performed test case 2 and we defer further discussion to Section 3.4.

### 3.3.5 Dependence of the results on the circumstellar discs

Returning to the evolution of the mass ratio and separation, although the overall agreement is good, there are two differences which need, briefly, to be commented on. These differences are related to the way in which the PBE and SPH codes handle the circumstellar discs.

First, S1 and S2 both give a slower rate of increase of the mass ratio initially than is predicted by the PBE code (Figure 3a;  $1 \leq M_{\text{acc}} \lesssim 2$ ). This reflects a problem with the SPH calculations rather than with the PBE code: namely, the size of the accretion radius around the secondary is initially of a similar size to that of the circumstellar disc which should form. This stops a circumsecondary disc from forming which reduces the secondary's cross-section for capturing infalling gas and, so, reduces the amount of gas captured by the secondary. Only when  $M_{\text{acc}} \gtrsim 2.0$ , is the specific angular

**Figure 4.** Snapshots of the evolution of test case 1 using the SPH code with artificial viscosity S2. The panels show the logarithm of column density, looking down the rotation axis, as the binary accretes infalling gas. The primary is on the right. The calculation starts when the mass accreted from the cloud is  $M_{\text{acc}} = 1$  and is followed until  $M_{\text{acc}} = 6$ . Notice that, initially, the circumsecondary disc is too small to be resolved and it only begins to be resolved when  $M_{\text{acc}} \gtrsim 2.0$ . Each panel has a width of twice the binary’s initial separation. Snapshots from calculations S1 and S2 look almost identical.

**Figure 5.** The same as in Figure 4, except using artificial viscosity B1 and only following the binary until  $M_{\text{acc}} = 5.0$ . With the different viscosity, the circumsecondary disc is unresolved for much longer (until  $M_{\text{acc}} \gtrsim 4.0$ ) and a circumbinary disc starts to form earlier at  $M_{\text{acc}} \approx 4.4$ . Each panel has a width of 4 times the binary’s initial separation.

momentum of the gas being captured by the secondary large enough for it to form a circumsecondary disc outside the accretion radius (Figure 4). From this point on, the mass ratio increases at the rate predicted by the PBE code. B1 has a similar problem, but for a slightly different reason. B1 has much less shear *and bulk* viscosity in shearing flows. In order for infalling gas to form a resolved disc around the secondary, it must, first, dissipate most of its kinetic energy so that it is captured by the secondary and, second, dissipate enough kinetic energy that the gas particles have roughly circular orbits. If the gas does not dissipate enough kinetic energy to be captured by the secondary on its first pass, it is likely to be captured by the primary instead which is deeper in the gravitational potential well. If a gas particle is captured

by the secondary but still has a very elliptical orbit, it will pass inside the secondary’s accretion radius and be removed. Thus, the low bulk viscosity of B1 means that the formation of a resolved circumstellar disc around the secondary is delayed until  $M_{\text{acc}} \gtrsim 3.9$  (Figure 5) and the cross-section of the secondary is underestimated until this point. As with S1 and S2, however, as soon as the circumsecondary disc is resolved ( $M_{\text{acc}} \gtrsim 3.9$ ), the mass ratio begins to increase at the rate predicted by the PBE code (Figure 3a).

Second, the PBE code does not include viscous evolution of the circumstellar discs. In reality, and in the SPH calculations, such viscous evolution results in the transfer of angular momentum from the discs to the orbit of the binary, increasing the separation.



In order for us to be able to neglect viscous evolution of the circumstellar discs, this transfer of angular momentum must be negligible over the time for most of the envelope to be accreted. Viscous evolution of the circumstellar discs on a longer time-scale may increase the final separation of the binary by a small factor, but the masses of the binary's components will have been determined during the accretion phase.

For wide binaries, viscous evolution is unlikely to be significant. For example, the free-fall time for a dense molecular cloud core ( $10^{-18} \text{ g cm}^{-3}$ ) is  $\sim 10^5$  years. The envelope will fall on to the binary on this time-scale. The viscous time for one of the circumstellar discs is of order

$$t_v \sim \frac{P}{2\pi\alpha_{SS}} \left(\frac{R}{H}\right)^2, \quad (20)$$

where  $P$  is the period of the binary,  $\alpha_{SS}$  measures the strength of the shear viscosity using the standard Shakura–Sunyaev prescription, and  $H/R$  is the ratio of the thickness of the disc to its radius (typically  $\sim 0.1$ ; Burrows et al. 1996; Stapelfeldt et al. 1998). Observationally, it is thought that the shear viscosity acting in protostellar accretion discs is of order  $\alpha_{ss} \sim 0.01$  (Hartmann et al. 1998). Thus, taking the median binary separation of 30 AU (Duquennoy & Mayor 1991) and a typical protobinary mass of  $0.1M_{\odot}$ , the viscous time in one of the circumstellar discs is  $\sim 10^6$  years, an order of magnitude longer than the free-fall time. For close binaries (separations  $\lesssim 5$  AU) viscous evolution may be expected to have some effect during the accretion phase. However, in most cases, a close binary is expected to have a circumbinary disc (see Section 6.5) and interactions between it and the binary will dominate the interactions between the circumstellar discs and the binary (Section 3.4.4).

In SPH calculations S1 and S2, viscous evolution of the circumstellar discs does affect the binary's separation during the calculation. For example, in calculation S1 when  $M_{\text{acc}} \gtrsim 3$ , the separation increases more rapidly than predicted by the PBE code and when  $M_{\text{acc}} = 6$ , after  $\approx 60$  orbits ( $\approx 4 \times 10^4$  years) the separation is 20% larger than predicted. However, we estimate (Pongracic 1988; Meglicki, Wickramasinghe & Bicknell 1993; Artymowicz & Lubow 1994) the effective viscosity in the circumstellar discs to be  $\alpha_{SS} \approx 0.2$ . With an orbital period of  $\approx 600$  years over most of the evolution, this gives a viscous time of  $\sim 5 \times 10^4$  years which is similar to the time over which the calculation was followed. Therefore, it is not surprising that the separation was affected. We note, however, that this viscosity is  $\approx 20$  times stronger than is expected in real protostellar discs and, thus, the effect on a real protobinary system over this period would have been negligible, as is assumed by the PBE code. Calculation S2 has approximately half the shear viscosity of S1 and its separation is correspondingly closer to the PBE code prediction. B1 has much less shear viscosity than S1 or S2. Consequently, the *rate of change* of separation when  $M_{\text{acc}} \gtrsim 3$  is very close to that predicted by the PBE code. Instead, with B1, the differences in the evolution of the separation occurred earlier in the evolution ( $1.5 \lesssim M_{\text{acc}} \lesssim 2.5$ ).

We conclude that it is reasonable for the PBE code to neglect the effect on the separation due to viscous evolution of the circumstellar discs since it is only likely to have a significant effect for close binaries and in these cases the effect is likely to be overwhelmed by the interaction between the

binary and a circumbinary disc. We also find that the small differences between the PBE and SPH results for the evolution of the mass ratio and separation reflect the unphysical treatment of the circumstellar discs by the SPH code rather than a problem with the PBE code.

### 3.3.6 Eccentricity evolution

Finally, we comment on the eccentricity of the binary as given by the SPH code. We see that initially, independent of the viscosity, the binary becomes eccentric due to the accretion of gas, with a peak eccentricity of  $e \approx 0.14$ . The eccentricity then displays a secular decrease, as the accretion rate on to the binary also decreases, while oscillating on an orbital time-scale. Such periodic changes of the orbital elements are known from analytic solutions of binary motion under a perturbing force (Kopal 1959), in this case, the accreting gas. Later in the evolution, the eccentricity displays a secular increase which depends on the shear viscosity in the calculations: the greater the shear viscosity, the earlier the increase begins. As with the overestimate of the rate of change of orbital separation that was given by S1 and S2 when  $M_{\text{acc}} \gtrsim 3$ , the eccentricity increases due to the unphysically-rapid transfer of angular momentum and energy from the circumstellar discs into the binary's orbit.

## 3.4 Test case 2

The second test case was chosen primarily to study the differences that appeared in test case 1 between the PBE and SPH codes regarding the formation of a circumbinary disc. A more centrally-condensed initial cloud results in the gas which first falls on to the binary having more specific angular momentum than with a uniform-density cloud and in a more rapid increase of the specific angular momentum of the gas as the accretion proceeds (see Section 4.2). Therefore, a circumbinary disc should form earlier than with test case 1 and provide us with a better test for the evolution of the circumbinary disc. The evolutions given by the PBE code and two different SPH calculations are given in Figure 6, with snapshots from the SPH calculations in Figures 7 and 8.

### 3.4.1 PBE calculation

The PBE code predicts that at the end of the evolution the mass ratio should have increased from  $q = 0.6$  to  $q \approx 0.88$  while the separation, after decreasing slightly at the beginning, finally ends up at  $\approx 2.3$  times the initial separation. The mass of the circumbinary disc becomes significant ( $M_{\text{cb}}/M_{\text{b}} \gtrsim 1/20$ ) at  $M_{\text{acc}} \approx 1.5$ , and at the end of the calculation the circumbinary disc contains  $\approx 13\%$  of the total mass.

### 3.4.2 SPH calculations

The SPH calculations had two different forms of artificial viscosity: B1: Balsara, with  $\alpha_v = 0.25$  and  $\beta_v = 1$ ; D1:  $\nabla \cdot \mathbf{v}$ , also with  $\alpha_v = 0.25$  and  $\beta_v = 1$ . Both formulations have low shear viscosity. The bulk viscosities are similar in non-shearing flows, but in shearing flows B1 has less bulk

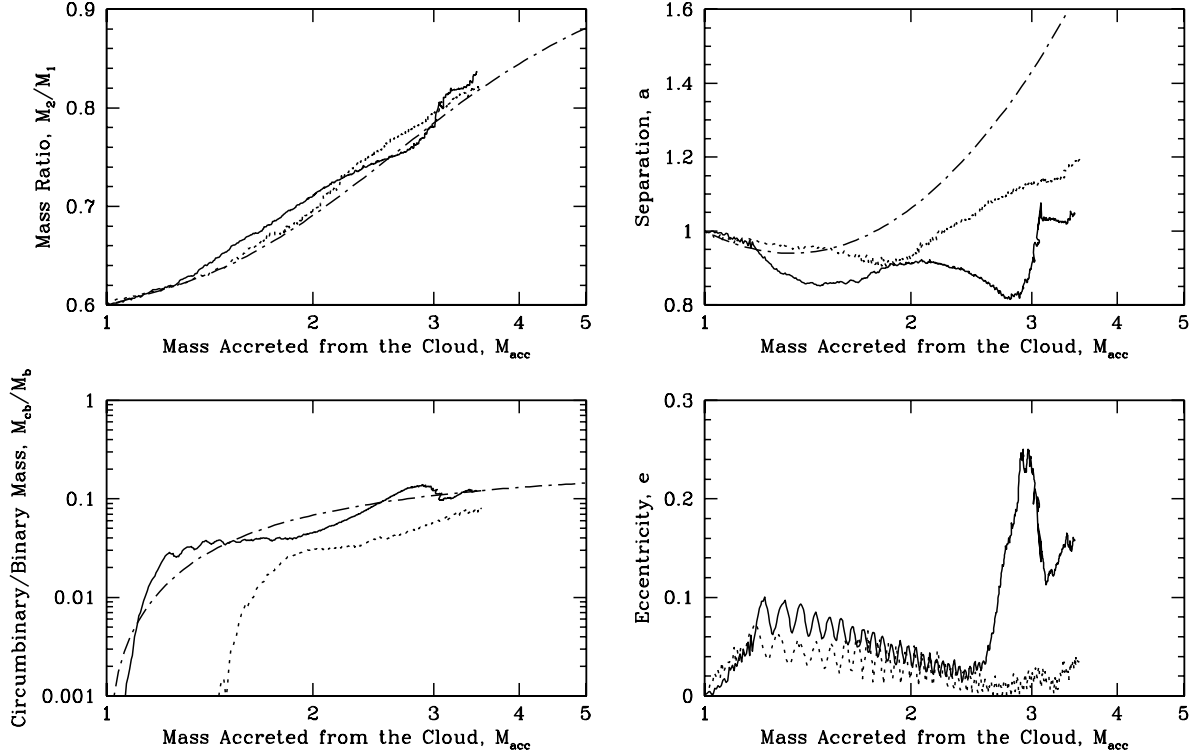


**Figure 6.** Second comparison of the results from the protobinary evolution (PBE) code with those from the full SPH calculations. The graphs show the evolution of a protobinary system that was formed in the centre of a collapsing molecular cloud core which initially had a  $1/r$ -density profile and was in solid-body rotation. The evolution of the (a; upper left) mass ratio, (b; upper right) separation, (c; lower left) ratio of mass in a circumbinary disc to that of the binary, and (d; lower right) eccentricity are plotted as the binary accretes gas from the infalling envelope. The dot-dashed lines show results from the PBE code. The other lines show the results from the full SPH calculations with artificial viscosities of B1 (dotted) and D1 (solid) (see Section 3.4.2).

viscosity. We do not use the Standard viscosity formulation (S1 or S2 in test case 1) because of our finding that its large shear viscosity inhibits the formation of a circumbinary disc and leads to rapid evolution of the circumstellar discs.

As with test case 1, due to the computational cost, the SPH calculations are stopped before all of the gas has fallen on to the binary. Each calculation took  $\approx 4$  months on a 300 MHz Sun Ultra workstation (using the binary tree, not a GRAPE board). During the calculations, the binaries performed  $\approx 60$  orbits and  $\approx 70\%$  of the total mass was accreted by the binary or settled into a circumbinary disc.

### 3.4.3 Evolution of the mass ratio

The agreement for the evolution of the mass ratio is even better than it was with test case 1 with differences of  $\lesssim 3\%$ . This is because, in this test case, the specific angular momentum of the gas being captured by the secondary is large enough for it to form a circumsecondary disc outside the accretion radius as soon as the SPH calculations begin, regardless of the viscosity (Figures 7 and 8). The SPH calculations generally give a slightly higher mass ratio than is predicted by the PBE code which is exactly what is expected because the PBE code ignores the separation-decreasing effect of the interaction between the binary and the circumbinary disc (a smaller binary separation means that the specific angular

momentum of the gas is higher relative to that of the binary, resulting in more gas being captured by the secondary).

### 3.4.4 Circumbinary disc evolution and interactions

For test case 2, the differences between the PBE and SPH results involve the formation of the circumbinary disc and its interaction with the binary, the latter of which is not accounted for in the PBE code. Generally, a binary will interact with a circumbinary disc so as to transfer angular momentum from its orbit into the gas of the circumbinary disc. This tends to decrease the separation of the binary and increase its eccentricity (Artymowicz et al. 1991; Lubow & Artymowicz 1996). Both these effects can be seen in the SPH calculations. The separation follows the prediction of the PBE code to better than 3% until the circumbinary disc begins to form, after which it is always smaller than predicted by the PBE code. As in test case 1, the eccentricity grows at the start of the calculation and then displays a secular decrease with time. However, when the mass of the circumbinary disc exceeds  $\approx 0.05M_b$ , the transfer of angular momentum from the binary to the circumbinary disc overwhelms the eccentricity-decreasing effect of the infalling gas and the eccentricity increases.

As with test case 1, different formulations of the SPH viscosity give slightly different evolutions. D1 results in earlier formation of a circumbinary disc than B1, although at

**Figure 7.** Snapshots of the evolution of test case 2 using the SPH code with artificial viscosity B1. The panels show the logarithm of column density, looking down the rotation axis, as the binary accretes infalling gas. The primary is on the right. The evolution starts when the mass accreted from the cloud is  $M_{\text{acc}} = 1$  and is followed until  $M_{\text{acc}} = 3.5$ . Two circumstellar discs are formed as soon as the calculation begins and a circumbinary disc begins to form at  $M_{\text{acc}} \gtrsim 1.4$ . Each panel has a width of 8 times the binary’s initial separation.

**Figure 8.** The same as in Figure 7, except using artificial viscosity D1. With the different viscosity, the circumbinary disc forms earlier (at  $M_{\text{acc}} \approx 1.1$ ) and the spiral shocks in the disc are better resolved.

$M_{\text{acc}} = 2$  and  $M_{\text{acc}} = 3.5$  the circumbinary disc masses only differ by  $\approx 30\%$ . More importantly, we find that B1 gives very poor resolution of spiral shocks in the circumbinary disc (created by gravitational torques from the binary) due to its lower bulk viscosity in shearing flows compared to D1 (c.f. Figures 7 and 8). The better shock resolution of D1 results in more efficient angular momentum transport from the binary’s orbit to the circumbinary disc which leads to a smaller binary separation and, consequently, more of the infalling gas settles into the circumbinary disc than with B1. This can be seen in the rapid decrease in separation of D1 compared to B1 when  $2.0 \lesssim M_{\text{acc}} \lesssim 2.6$  (Figure 6b), and, simultaneously, the more rapid increase in the mass of the circumbinary disc for D1 (Figure 6c).

From the point of view of the ability to resolve shocks in the circumbinary disc, D1 is more realistic than B1 and we emphasise that extreme care should be used when employing the Balsara formulation of viscosity in shearing flows. Given that D1 appears to give more realistic results than B1, is it encouraging to note that over the entire evolution the PBE code predicts the circumbinary disc mass to within a factor of 2 of that given by the D1 SPH calculation (Figure 6).

### 3.5 Conclusions and limitations of the PBE code

In summary, in the absence of a massive circumbinary disc, the PBE code gives results which are in good qualitative and quantitative agreement with the full hydrodynamic calculations. In all cases, the binary’s mass ratio is predicted to within 5% of the SPH results *over an increase in the binary’s total mass by a factor of up to 6!* In test case 1, the binary’s separation is predicted to within 20% by the PBE code. Furthermore, in test case 1, even these small dif-

ferences can be attributed to the SPH code’s inability to resolve the circumsecondary disc during parts of the calculations or unphysically-rapid viscous evolution of the circumstellar discs, rather than a problem with the PBE code. Thus, **the results from the PBE code are at least as accurate as those given by a full SPH calculation, but the PBE code is  $\sim 10^6$  times faster.** This makes it possible to investigate the statistical properties of binary stars (see the next section).

In cases where a circumbinary disc forms around the binary, the PBE code generally predicts that the disc forms earlier than in the full SPH calculations, especially in the more borderline case of a progenitor molecular cloud core with uniform-density. However, in the best case for studying the formation of a circumbinary disc (test case 2, D1) the time of formation of the circumbinary disc was in good agreement and its mass was predicted to within a factor of 2 throughout the evolution.

The main omission in the PBE code is that, if a massive circumbinary disc is formed ( $M_{\text{cb}}/M_{\text{b}} \gtrsim 1/20$ ), the code ignores the interaction between it and the binary. Omitting this interaction leads to the separation of the binary being *overestimated* by the PBE code. From the SPH results, we find that **if a massive circumbinary disc is formed, the binary’s separation is likely to remain approximately constant as it accretes from a gaseous envelope.** The overestimate of the separation by the PBE code means that **the mass of the circumbinary disc is likely to be underestimated and, for the same increase in the binary’s mass, the binary’s mass ratio will be underestimated.** We note, however, that this omission serves only to *strengthen* the predictions of the properties of binary stars that we obtain in Section 6.

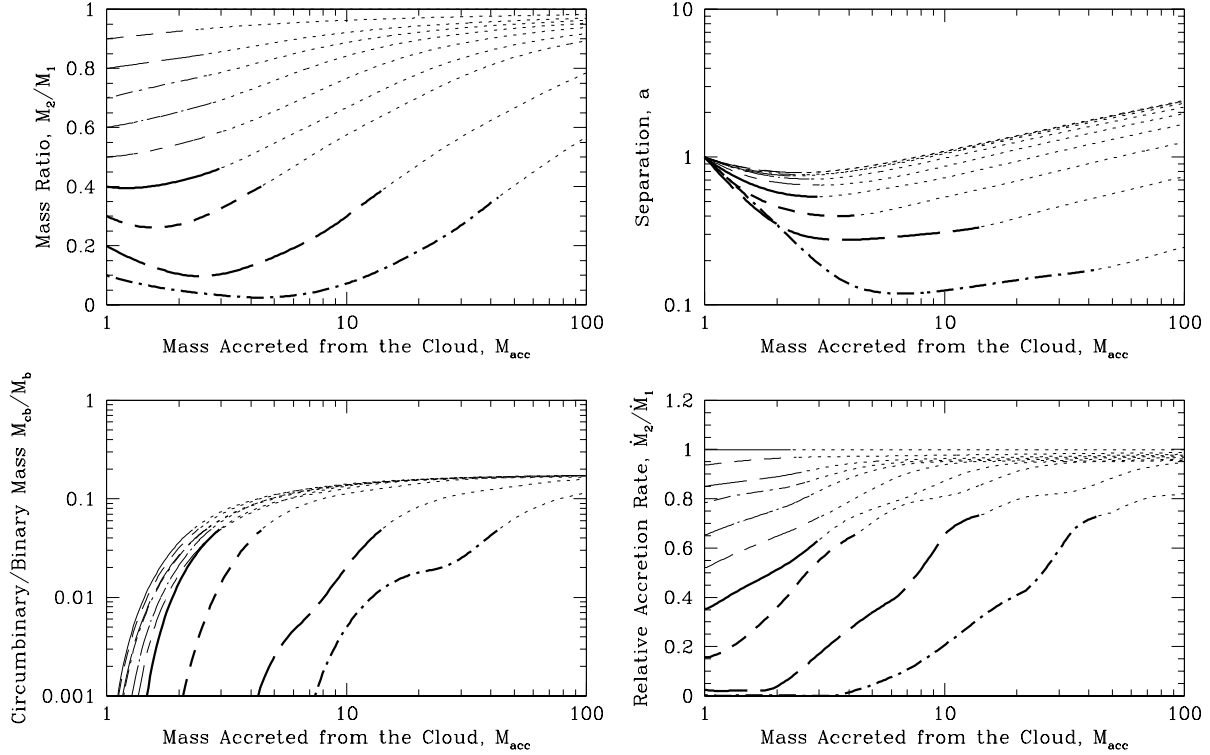


**Figure 9.** The evolution of protobinary systems which were formed in the centres of collapsing molecular cloud cores as they accrete from their gaseous envelopes. The initial cores have uniform-density profiles and are in solid-body rotation. The evolution of the mass ratio (a; upper left), separation (b; upper right), and ratio of the circumbinary disc mass to that of the binary (c; lower left), and the relative accretion rate (d; lower right) are given as functions of the amount of gas that has been accreted from the envelope. The evolutions are given for binary systems with initial mass ratios of  $q = 0.1$  to  $q = 1.0$ , with various different line types and/or line widths for each. The functions are all given by thin dotted lines once the circumbinary disc mass exceeds 5% of the binary’s mass. Beyond this point, the binary’s mass ratio and the mass in the circumbinary disc are likely to be underestimated, and the separation is likely to be overestimated. Masses are given in units of the binary’s initial mass; separation is given in units of the binary’s initial separation.

#### 4 PROTOBINARY EVOLUTION

We now use the PBE code to study the evolution and final states of binaries that are formed from the collapse of 6 types of molecular cloud core. We study binaries that are formed from clouds with three different initial density profiles: uniform-density, and power-law profiles of  $\rho \propto 1/r$  and  $\rho \propto 1/r^2$  (i.e.  $\lambda=0, -1$ , and  $-2$ ). For each of these three density profiles, we study two different initial rotation profiles: solid-body rotation, and  $\Omega_c \propto 1/r$  (i.e.  $\beta=0$ , and  $-1$ ).

These initial conditions are highly idealised. However, we use them to illustrate how the properties of a binary depend on the degree of central condensation and the amount of differential rotation in its progenitor molecular cloud core. In fact, in several cases the initial conditions represent extremes; the initial conditions before dynamic collapse occurs are almost certainly somewhat centrally-condensed, but are almost certainly less centrally condensed than  $\rho \propto 1/r^2$ . In Section 6, we use the conclusions reached from these calculations to predict the properties of binaries and to constrain the properties of the molecular cloud cores from which they formed.

For each type of cloud (Figures 9 to 13), we consider the evolution of ‘seed’ binaries that form with initial mass ratios in the range  $0.1 \leq q \leq 1.0$ . We give the mass ratio  $M_2/M_1$ , separation  $a$ , ratio of the mass of the circumbinary

disc compared to the binary’s mass  $M_{cb}/M_b$ , and relative accretion rate  $\dot{M}_2/\dot{M}_1$ , as functions of the total mass that has fallen on to the binary system from the envelope,  $M_{acc}$ . As mentioned in Section 2.1, the figures that are produced can be viewed in two ways: either as giving the *evolution of individual protobinary systems* as they evolve from their initial mass ( $M_{acc} = M_b = 1$ ) to a higher total mass (up to  $M_{acc} = 100$ ), or, for the first three panels in each figure, as giving the *final states* of binaries that initially began with masses ranging from 1% ( $M_{acc} = 100$  when the accretion stops) to 100% ( $M_{acc} = 1$  if there is no accretion on to the protobinary) of the cloud’s total mass  $M_c$ .

##### 4.1 Solid-body rotation, uniform-density profile

Figure 9 gives the results for binaries formed from initially uniform-density clouds in solid-body rotation. The long-term evolution of the mass ratios is that they increase toward unity (equal mass components). The separation initially decreases, due to accretion of gas with low mean specific angular momentum, but increases in the long-term. Both of these long-term effects are a consequence of the fact that the specific angular momentum of the infalling gas increases quickly as mass is accreted (Figure 2), since the accretion of material with high specific angular momentum increases

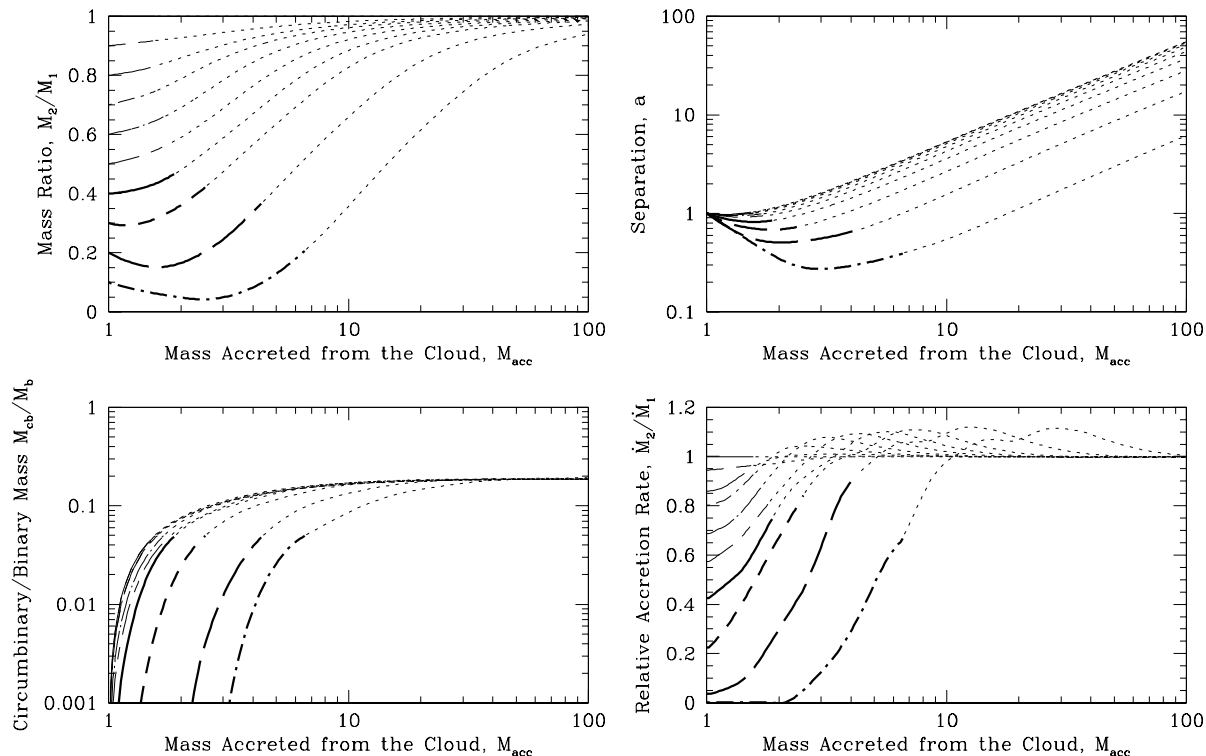


**Figure 10.** The evolution of protobinary systems which were formed in the centres of collapsing molecular cloud cores as they accrete from their gaseous envelopes. The initial cores have *either*  $1/r$ -density profiles and are in solid-body rotation, *or*  $1/r^2$ -density profiles and are in differential rotation with  $\Omega_c \propto 1/r$ . These two types of core have the same relationship between angular momentum and mass (see Figure 2). See Figure 9 for a description of the plots.

the mass ratio and separation, while the accretion of material with low specific angular momentum decreases both the mass ratio and separation (Artymowicz 1983; Bate 1997; Bate & Bonnell 1997).

The different evolutions for the different ‘seed’ mass ratios are in large part due to the way we have chosen the initial conditions (Section 2.1). We assumed that the central region of the progenitor cloud from which the ‘seed’ binary formed had the same angular momentum as that contained in the orbit of the ‘seed’ binary (equation 3). For a ‘seed’ binary with a given mass ratio and separation these initial conditions give the slowest possible rotation rate of the progenitor core and, therefore, the *slowest possible evolution toward equal mass ratios and the formation of circumbinary discs*. However, they also mean that the gas which is accreted by a ‘seed’ binary with a low mass ratio has *less* specific angular momentum than for a binary with a high mass ratio. Hence, the mass ratio of a ‘seed’ binary with a small mass ratio tends to decrease initially, while that of a binary with a large mass ratio tends to increase.

This dependence of the rotation rate of the progenitor cloud on the mass ratio of the ‘seed’ binary also largely explains why the evolution of the separation (Figure 9b) and circumbinary disc (Figure 9c) differ for different initial mass ratios. In all cases, the separation decreases initially, but it does so quicker and for longer in systems with smaller initial mass ratios because the specific angular momentum of the infalling gas is lower. Likewise, the formation of a circumbinary disc requires more accretion for systems with

lower initial mass ratios. However, for the formation of a circumbinary disc, there is an additional effect. For a system with a low mass ratio, the secondary is at a larger radius from the binary’s centre of mass than in a system with a high mass ratio. Therefore, the infalling gas must have more specific angular momentum before it can form a circumbinary disc rather than be captured by the secondary.

In all cases, the long-term evolution is that the binary reaches a steady-state in which a constant fraction of the infalling gas is captured by the binary with the rest going into the circumbinary disc and  $\dot{M}_{cb}/\dot{M}_b \approx 0.17$ . Since the specific angular momentum of the gas that falls on to the binary is always increasing (Figure 2), this indicates that a steady-state is established in which the binary continually adjusts to the accretion so that ratio of the specific angular momentum of the infalling gas to  $\sqrt{GM_b a}$  (which is related to the specific angular momentum of the binary) is constant (see equation 5). Of course, as shown by the test calculations (Section 3), when the circumbinary disc becomes massive ( $M_{cb}/M_b \gtrsim 1/20$ ; dotted lines in Figures 9 to 14) the interaction of the binary with the disc will not allow this same equilibrium to be established. Instead the separations will be lower and more of the infalling gas will settle into the circumbinary disc than is predicted here. In addition, for the same increase in the mass of the binary, the mass ratio will tend to increase even more rapidly toward equal mass protostars because the smaller separation of the binary means that the specific angular momentum of the gas compared to that of the binary will be somewhat larger. Thus,

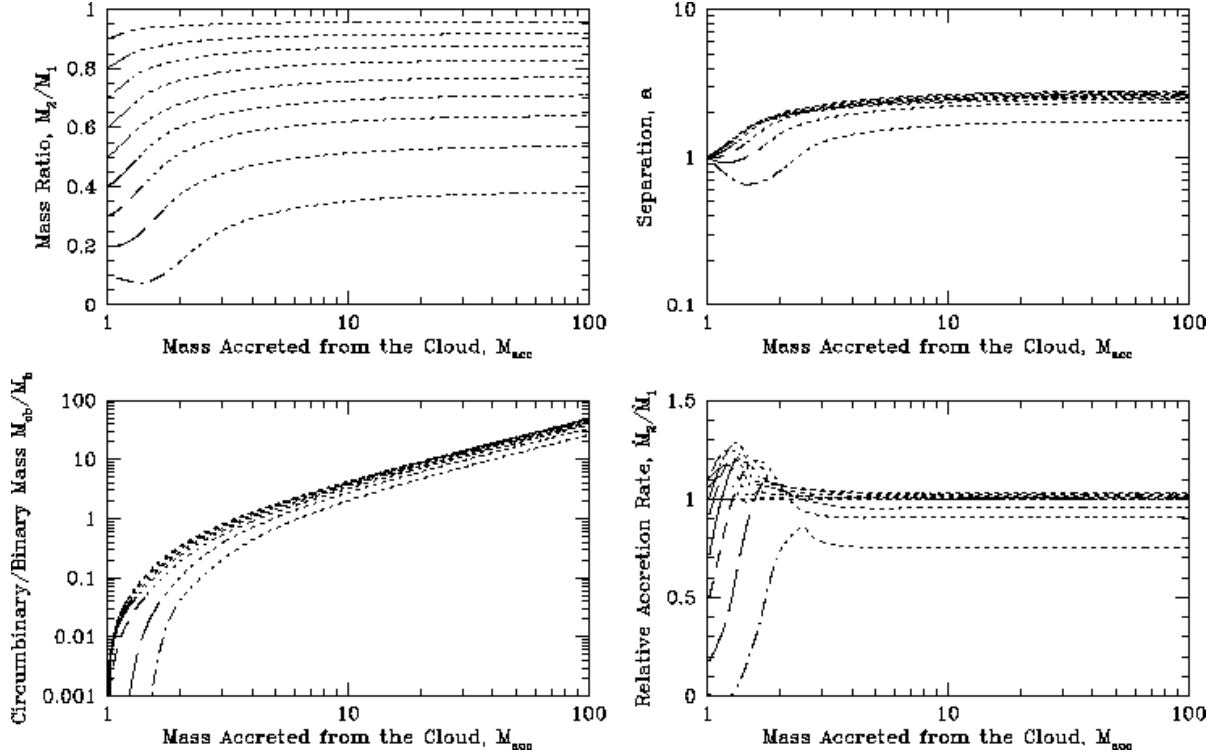


**Figure 11.** The evolution of protobinary systems which were formed in the centres of collapsing molecular cloud cores as they accrete from their gaseous envelopes. The initial cores have  $1/r^2$ -density profiles and are in solid-body rotation. The binaries rapidly evolve to a state where most of the infalling gas accumulates in a massive circumbinary disc and the binary itself ceases to evolve. See Figure 9 for a description of the plots.

as with the assumption that the cloud rotates at the slowest possible rate, *ignoring the interaction of the binary with the circumbinary disc gives the slowest possible evolution toward equal masses and the formation of a massive circumbinary disc.*

#### 4.2 Solid-body rotation, $1/r$ -density profile

Figure 10 gives the results for binaries formed from progenitor clouds with  $1/r$ -density profiles in solid-body rotation. The evolutions are similar to the uniform-density calculations, but everything evolves toward high-angular-momentum behaviour after the accretion of less gas. The mass ratios evolve toward unity and a massive circumbinary disc is formed after less mass has been accreted. The separations begin increasing earlier, and increase by a greater amount for the same amount of accretion.

The more rapid evolution toward high-angular-momentum behaviour than with the uniform-density cloud is because the infalling gas has a more specific angular momentum initially, and its specific angular momentum increases more rapidly with mass (Figure 2). This also means that, to reach a steady-state, the binary must increase  $\sqrt{GM_b a}$  more rapidly. Hence, a steady-state is attained when the infalling gas has more specific angular momentum relative to the binary than in the uniform-density case, and thus  $\dot{M}_{cb}/\dot{M}_b$  is also higher at  $\approx 0.19$ . Again, however, the interaction of the binary with the circumbinary disc, which is not taken into account by the PBE code, is likely to lead

to: significantly smaller separations; more mass in the circumbinary disc; and, for a given increase in the binary's total mass, a mass ratio that is even closer to unity.

#### 4.3 Solid-body rotation, $1/r^2$ -density profile

Figure 11 gives the results for binaries formed from progenitor clouds with  $1/r^2$ -density profiles in solid-body rotation. The rate of increase of the specific angular momentum of the gas as mass is accreted is now so rapid (Figure 2) that the binary cannot evolve fast enough to keep up with it. This results in the rapid formation and runaway growth of a massive circumbinary disc (Figure 11c) because the infalling gas has too much angular momentum to be captured by the individual components of the binary. The binary only accretes a maximum of 1 – 3 times its initial mass, even if the cloud mass is 100 times the initial binary mass – the rest of the gas goes into the circumbinary disc.

Of course, in reality, if the circumbinary disc becomes comparable in mass to the binary we would expect it to react in ways that are not possible to follow with the simple PBE calculations. Interaction between the binary and circumbinary disc could lead to two possibilities. First, the disc may fragment to form one or more additional protostellar objects (e.g. Bonnell & Bate 1994a; Burkert & Bodenheimer 1996; Burkert et al. 1997). In this case, the model has completely broken down, since in this paper we assume that a binary is formed by an initial binary fragmentation and subsequent accretion. There is no allowance made for additional frag-

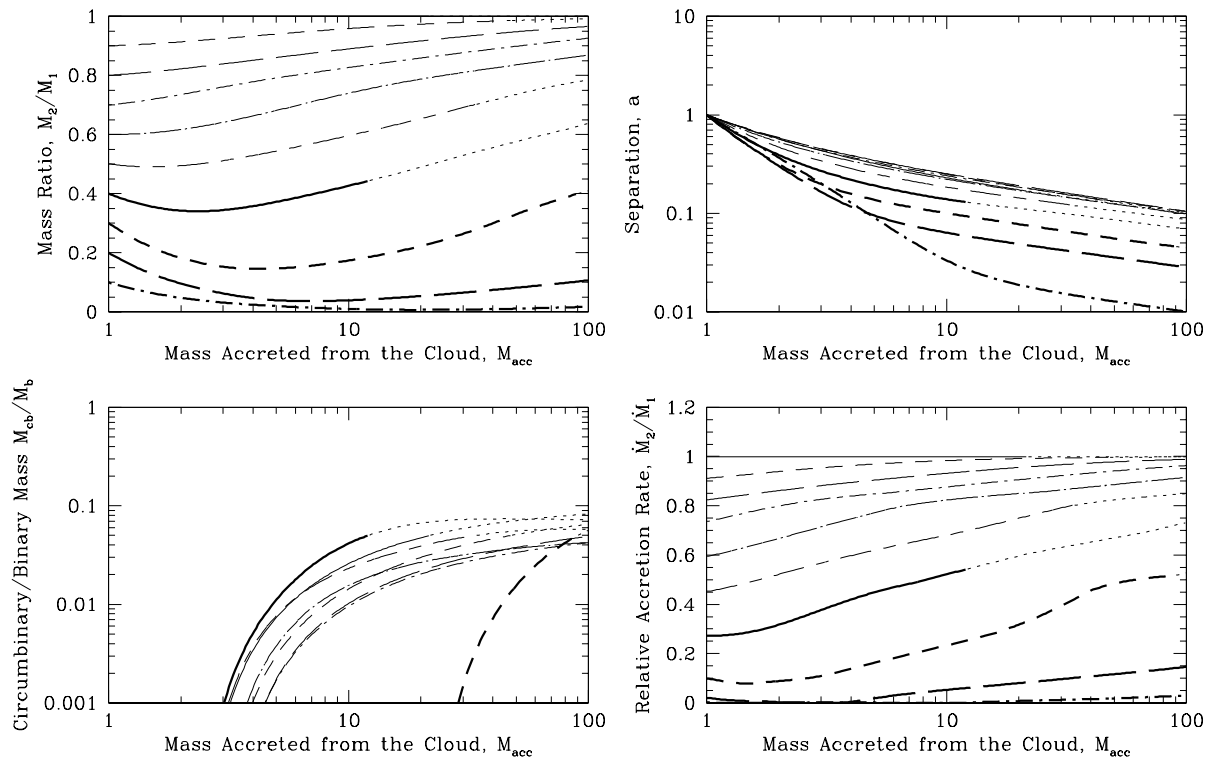


**Figure 12.** The evolution of protobinary systems which were formed in the centres of collapsing molecular cloud cores as they accrete from their gaseous envelopes. The initial cores have uniform-density profiles and differential rotation of  $\Omega_c \propto 1/r$ . See Figure 9 for a description of the plots.

mentation. The second possibility is that gas is accreted by the circumstellar discs of the two protostars from the circumbinary disc (Artymowicz & Lubow 1996; Lubow & Artymowicz 1996). If such accretion occurs, the binary’s mass ratio will inevitably evolve rapidly toward unity because this material has high specific angular momentum and will preferentially be captured by the secondary. The mass ratios would continue to follow the rapid increases seen early in Figure 11a (when  $M_{\text{acc}} \lesssim 2$ ), giving even faster evolution toward equal masses than was seen for cores with  $1/r$ -density profiles.

#### 4.4 Differential rotation, uniform-density profile

Figure 12 gives the results for initially uniform-density clouds in differential rotation with  $\Omega_c \propto 1/r$ . The specific angular momentum of the infalling gas is low to begin with and only slowly increases as mass is accreted (Figure 2). Thus, a binary’s mass ratio takes longer to evolve toward unity, the separation continually decreases, and a circumbinary disc takes longer to form than in the solid-body case (Figure 9). Even after a binary has accreted 100 times its initial mass, its mass ratio depends primarily on its initial value (Figure 12a). The ratio of the mass in the circumbinary disc to the binary’s mass is always less than 0.1, and in most cases less than 0.05, even after the infall of 100 times the binary’s initial mass.

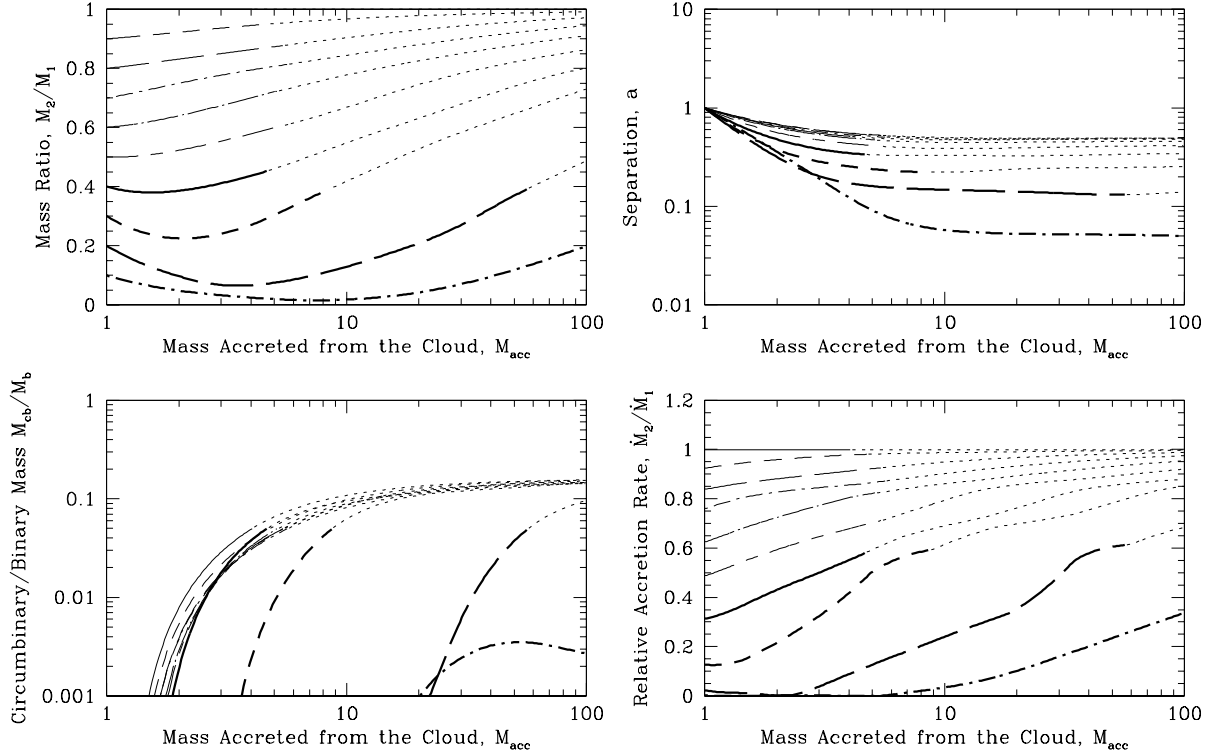
#### 4.5 Differential rotation, $1/r$ -density profile

Figure 13 gives the results for clouds with  $1/r$ -density profiles that are in differential rotation with  $\Omega_c \propto 1/r$ . Again, with differential rotation, the infall of gas with low specific angular momentum is maintained for longer than with solid-body rotation. The mass ratios do all increase toward unity after more than 10 times the binary’s initial mass has fallen in, however, after 100 times the initial binary’s mass has fallen in, a full range of mass ratios is still possible. The formation of a circumbinary disc is again delayed with differential rotation, although in most cases a steady-state is reached eventually with  $M_{\text{cb}}/M_b \approx 0.15$ .

#### 4.6 Differential rotation, $1/r^2$ -density profile

Finally, we consider the evolution of binaries formed from progenitor clouds with  $1/r^2$ -density profiles that are in differential rotation with  $\Omega_c \propto 1/r$ . From Figure 2, the relationship between angular momentum and mass in the progenitor cloud is identical to a cloud with a  $1/r$ -density profile in solid-body rotation and, therefore, the evolution is identical to that in Figure 10.

Compared to  $1/r^2$ -density with solid-body rotation, the effect of differential rotation is, once again, to decrease the rates of increase of the mass ratio and separation (at least while the binary is still accreting gas in Figure 11), and to delay the formation of a circumbinary disc. The reduced rate of increase of the specific angular momentum of the infalling gas means that, unlike in the case with solid-body



**Figure 13.** The evolution of protobinary systems which were formed in the centres of collapsing molecular cloud cores as they accrete from their gaseous envelopes. The initial cores have  $1/r$ -density profiles and differential rotation of  $\Omega_c \propto 1/r$ . See Figure 9 for a description of the plots.

rotation, the binary can reach an equilibrium with the cloud; the runaway of the mass in the circumbinary disc is avoided. However, even such strong differential rotation is not enough to stop the mass ratios being driven toward unity with an initial density profile of  $\rho \propto 1/r^2$ .

## 5 RELAXING SOME OF THE ASSUMPTIONS

### 5.1 The rotation rate of the progenitor cloud

In the previous section, we assumed that the orbital angular momentum of the ‘seed’ binary system,  $L_b$ , was equal to the angular momentum of the spherical central region of the cloud,  $L_{cen}$ , from which the ‘seed’ binary formed (equation 3). This assumption gives a *lower limit* to the rate of rotation of the progenitor cloud, since it does not allow for the possibility of circumstellar discs around the ‘seed’ binary which would contain additional angular momentum. Furthermore, if the ‘seed’ binary was formed via fragmentation of a circumstellar disc surrounding a single protostar, then the disc must have had a radius at least as big as the separation of the ‘seed’ binary which forms (i.e. at least some gas in the disc must have had a specific angular momentum of  $j = \sqrt{GM_b a}$ ). Thus, some of the gas which falls on to the system from the envelope immediately after the ‘seed’ binary forms is expected to have at least this much specific angular momentum. As a comparison, the first gas to be accreted by the binaries in Figure 9 had at most 0.21 – 0.63 of this value, depending on the initial mass ratios. Therefore,

it is conceivable that the progenitor clouds may be rotating faster than we assumed in the previous section.

To demonstrate the effect of the progenitor cloud having a greater rate of rotation, we performed calculations which evolved binaries whose progenitor clouds were rotating rapidly enough that some (that part of the envelope which is in the plane of the binary) of the first gas to fall on to the binary had a specific angular momentum of  $j = \sqrt{GM_b a}$ . Thus, rather than setting  $R_b^2 \Omega_{Rb}$  using equation 3, we set

$$R_b^2 \Omega_{Rb} = \sqrt{GM_b a}, \quad (21)$$

*regardless of the initial mass ratio of the binary.* Thus, all the progenitor clouds have the same initial density profile and rotation rate and all the ‘seed’ binaries have the same separation, regardless of the mass ratio of the ‘seed’ binary. This also allows us to examine the degree to which the evolution of a binary depends on its mass ratio, and how much it depends on the properties of the gas which it accretes from the infalling envelope. These ‘seed’ binaries could have formed via the fragmentation of a disc, where we assume that the angular momentum that is in excess of the ‘seed’ binary’s orbital angular momentum,  $L_b$ , is contained in circumstellar discs.

The results for an initially uniform-density cloud in solid-body rotation are given in Figure 14. Due to the greater rotation rate of the progenitor cloud and, hence, the higher specific angular momentum of the gas which falls on to the binary, the mass ratios are driven toward unity after much less mass has been accreted compared with when the slow-



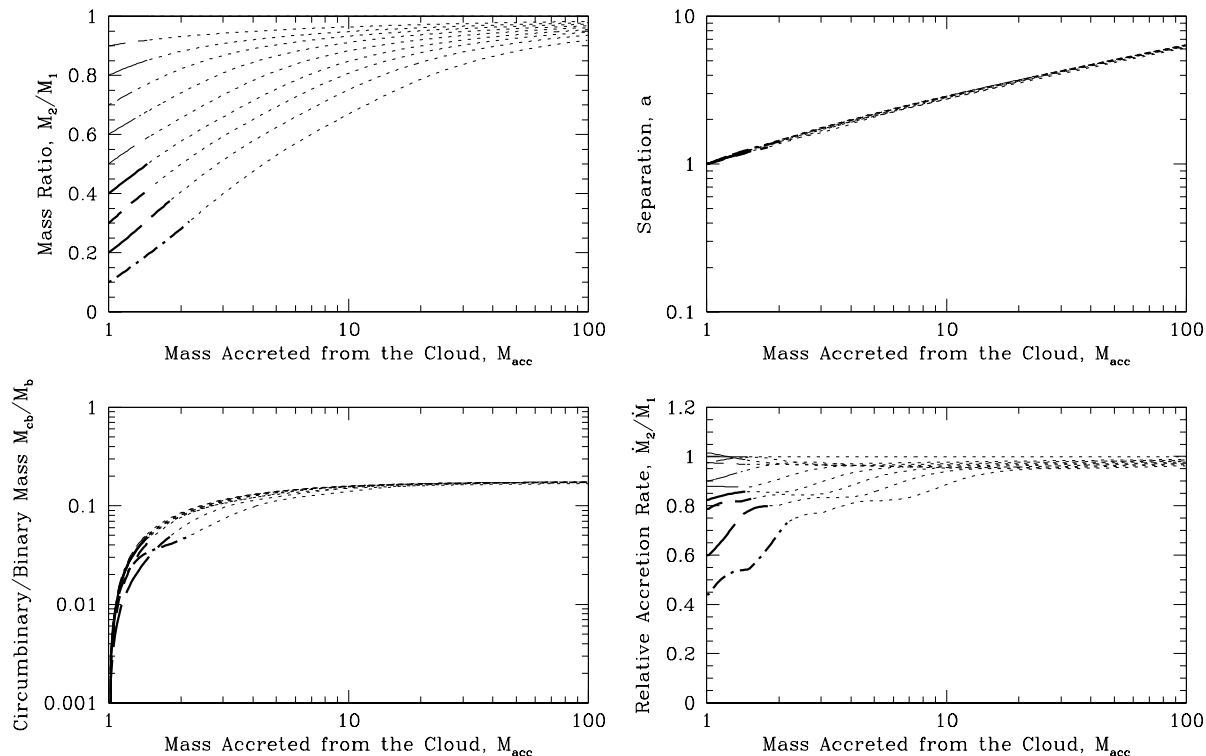


**Figure 14.** The evolution of protobinary systems which were formed in the centres of collapsing molecular cloud cores as they accrete from their gaseous envelopes. As in Figure 9, the initial cores have uniform density profiles and are in solid-body rotation, but here the clouds are rotating more rapidly and are all rotating at the same rate, regardless of the binary’s initial mass ratio (see Section 5.1). This type of evolution is appropriate for binaries that form via the fragmentation of a massive circumstellar disc surrounding single protostar. See Figure 9 for a description of the plots.

est possible rotation rate was used (Figure 9). Thus, **the rates of increase toward mass ratios of unity that are given in Section 4 are lower limits.**

In contrast to the previous section, the evolutions of the separation and the mass in a circumbinary disc are quite independent of the mass ratio of the binary, demonstrating that **the evolution of a binary’s separation and the formation of a circumbinary disc depend almost entirely on the properties of the infalling gas; the mass ratio of the binary has almost no effect.** The very small dependence of the mass of the circumbinary disc on the binary’s mass ratio is because the secondary is farther from the centre of mass in a binary with a lower mass ratio.

## 5.2 Different density profiles

The evolutions presented in Section 4 are for idealised progenitor cloud cores with power-law density and rotation profiles. These clearly illustrate the main dependencies of the evolution of a protobinary system as it accretes to its final mass. However, the PBE code easily be applied to other types of progenitor cloud core. For example, we have performed evolutions beginning with Gaussian centrally-condensed cores with inner to outer density contrasts of 20:1. These have density profiles that are similar to observed pre-stellar molecular cloud cores in that they are steep on the outside and flatter near the centre (Ward-Thompson et al. 1994; André, Ward-Thompson, Motte 1996; Ward-

Thompson, Motte, & André 1999). As one might expect, the evolutions lie between those for uniform-density clouds and those with  $\rho \propto 1/r$ , although they are closest to the uniform-density case.

## 5.3 Eccentric binary systems

In this paper, strictly, we only consider the evolution of protobinary systems with circular orbits. However, in the test cases of Section 3, where we compared the evolution given by the PBE code with those from full SPH calculations, we obtained good agreement even though the orbit of the binary in the SPH calculation had eccentricities up to  $e \approx 0.2$ . Therefore, we are confident that the results in this paper are valid for binaries with eccentricities  $e \lesssim 0.2$ .

For larger eccentricities, we expect the evolution of the binaries should be **qualitatively similar** to what we have found for circular binaries. Hence, we still expect that the long-term effect of accretion will be to drive the mass ratios toward unity and form circumbinary discs and that this evolution will be enhanced with more centrally-condensed initial conditions and diminished by differential rotation.

However, there will be quantitative differences. Most importantly, the formation of a circumbinary disc will be delayed in an eccentric system for two reasons. First, for the same semi-major axis, an eccentric binary has less angular momentum than a circular one and, thus, the gas from which it first formed (and hence the molecular cloud core as

a whole) may have been rotating more slowly. This would also mean that more gas is able to be accreted before the binary's mass ratio is driven toward unity. Second, for binaries with the same semi-major axis separation, a circumbinary disc must be formed at a larger radius from the centre of mass for an eccentric binary than for a circular binary to avoid disruption (e.g. Artymowicz & Lubow 1994). Thus, eccentric systems are expected to be able to accrete significantly more material than circular binaries before forming a circumbinary disc.

Other effects may include collisions between the protostars and their circumstellar discs (e.g. Hall, Clarke & Pringle 1996) and, of course, the eccentricity itself is expected to evolve due to accretion and the interactions between the protostars and the discs. These effects are beyond the scope of this paper, but would certainly be well worth studying.

## 6 THE PROPERTIES OF BINARY SYSTEMS

The aim of this paper is to determine, for a particular model of binary star formation, the properties of binaries and how they depend on the initial conditions in their progenitor molecular cloud cores. By comparing these predictions with observations, we hope to determine whether this is a viable model for binary star formation and, if so, to constrain the initial conditions for binary star formation. In order to do so, however, we must first discuss the relationship that is expected between the mass of a 'seed' binary system and its separation.

### 6.1 Dependence of the mass of a 'seed' protobinary on its separation

In this paper, we consider the evolution of a 'seed' binary system as it accretes gas from an infalling envelope, but we do not specify exactly how the protobinary is formed. Presumably, it is formed via some sort of fragmentation process (see Section 1). In order for binary fragmentation to occur, the Jeans radius at the time of fragmentation must be less than or approximately equal to the separation of the protobinary that is formed. Thus,  $a \gtrsim 2R_J$ , where  $R_J$  is the Jeans radius

$$R_J \approx \frac{2GM_{\text{frag}}\mu}{5R_g T}, \quad (22)$$

$\mu$  is the mean molecular weight, and  $R_g$  is the gas constant. The 'seed' binary's initial mass is approximately twice the mass of each fragment,  $M_{\text{frag}}$ . Therefore, for a constant temperature,  $T$ , we expect a roughly linear relationship between the mass of a 'seed' binary and its separation:  $M_b \approx 2M_{\text{frag}} \propto a$ .

Figure 15 gives the initial mass of a binary versus its separation from a series of fragmentation calculations performed by Boss (1986). Indeed, there is a strong, approximately linear, relationship between the binary's mass and its separation.

Using equation 22, we plot (solid line) the relationship if  $a = 2R_J$ . We use  $\mu = 2.46$  with  $T = 10$  K for densities below  $10^{-13}$  g cm $^{-3}$  and  $T \propto \rho^{\gamma-1}$  with  $\gamma = 1.4$  for  $10^{-13} \leq \rho < 6 \times 10^{-8}$  g cm $^{-3}$  and  $\gamma = 1.1$  for  $\rho \geq 6 \times 10^{-8}$

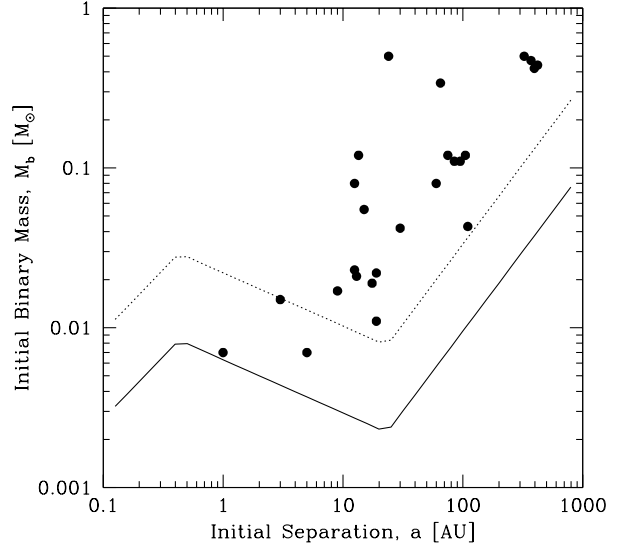


**Figure 15.** The dependence of a protobinary's initial mass on its separation. The points give the results from 26 fragmentation calculations (Figure 13, Boss 1986). The solid and dotted lines give simple estimates (see Section 6.1) of the minimum mass that a 'seed' protobinary system should have as a function of its separation.

g cm $^{-3}$  (e.g. Tohline 1982). The numerical results generally lie above the solid line because the properties of the binaries were calculated somewhat after they first began to form and they have already accreted some gas. For example, if we assume that the fragments are embedded in a sphere of gas with radius  $2R_J$  and a mean density of half the mean density of the fragments which is rapidly accreted by the fragments, then we obtain the dotted line for the masses of the 'seed' binaries. Furthermore, the fragments typically form on elliptical orbits and are initially falling toward each other (which moves the numerical results to smaller separations).

Generally, for separations  $\gtrsim 10$  AU, wider 'seed' binaries have larger initial masses, while for separations  $\lesssim 10$  AU the initial masses are  $\approx 0.01M_\odot$ . Therefore, for example, in order to form binary systems with a solar-mass primary, close systems ( $\lesssim 10$  AU) may have to accrete  $\sim 100$  times their initial mass. Systems with separations  $10 \lesssim a \lesssim 100$  AU need to accrete between 100–10 times their initial mass, and the widest systems need only accrete a few times their initial mass.

This leads us to our first prediction: for binary systems with the same total mass, **the properties of close systems will be more heavily determined by accretion than those of wide systems.** In turn this means that the mass ratios of wide binary systems are expected to be determined primarily from the initial density structure in the molecular cloud cores and so they may enable us to better understand the initial conditions for star formation by giving us a way to measure the density structure. Therefore, **in order to study the initial conditions for star formation we should consider the properties of wide binaries, while to learn more about the evolution due to accretion it is best to consider close binaries.**

A further prediction is: **if high and low mass stars form by the same general process, and the initial**

mass of a ‘seed’ binary is independent of the mass of the progenitor core, then the properties of massive binary systems should be more heavily influenced by accretion than those of lower mass systems with the same separation.

## 6.2 Binary mass ratios

In sections 4 and 5, we found that **the long-term evolution of an accreting binary is for its mass ratio to approach unity.**

### 6.2.1 Dependence of the mass ratio on separation

As argued in Section 6.1, for molecular cloud cores of a given mass, the amount of mass accreted by a binary, relative to its initial fragmentation mass, will be greater for close binaries than for wide systems. Thus, **closer binary systems are more likely to have mass ratios near unity than wider systems with the same total mass.**

Duquennoy & Mayor (1991) surveyed main-sequence G-dwarf stellar systems. They found that the mass ratio distribution, averaged over binaries with all separations, increases toward small mass ratios. However, there is mounting evidence that the mass-ratio distributions differ between short and long-period systems with the distribution for close binaries ( $P < 3000$  days;  $a \lesssim 5$  AU) consistent with a uniform distribution (Mazeh et al. 1992; Halbwachs, Mayor & Udry 1998). Thus, relative to wide systems, the close systems are biased toward mass ratios of unity, in agreement with the above prediction.

The fraction by which the mass of a ‘seed’ binary must be increased in order for its mass ratio to approach unity depends on the conditions in the progenitor cloud core. In general, **the less centrally-condensed a core is and/or the more differential rotation it has ( $\beta \leq 0$ ), the easier it is to form binary systems with low mass ratios for a given increase in the binary’s initial mass.** By inquiring how easy it is to reproduce the observed mass-ratio distributions with different types of progenitor molecular cloud core, we can use these results to constrain the initial conditions for binary star formation.

Duquennoy & Mayor (1991) found that binaries containing G-dwarfs with separations  $\gtrsim 30$  AU generally have unequal mass ratios (typically  $q \approx 0.3$ ). From Figure 15, typically, these binaries may be expected to accrete  $\sim 10$  times their ‘seed’ mass. For uniform-density progenitor clouds in solid-body rotation (Figure 9a), this observed mass ratio distribution could be produced if the fragmentation process typically produces ‘seed’ binaries with low mass ratios ( $q \approx 0.2$ ). However, with more centrally-condensed cores it becomes progressively more difficult to produce the observed mass-ratio distribution because the accretion drives the initial mass ratios toward unity (Figures 10a and 11a). With  $\rho \propto 1/r$  cores, the ‘seed’ binaries must typically have mass ratios of  $q \approx 0.1$  in order to produce G-dwarf binaries that have typical mass ratios of  $q \approx 0.3$ . With  $\rho \propto 1/r^2$  (assuming the ‘seed’ binaries manage to accrete from their circumbinary discs) it is difficult to see how the observed mass-ratio distribution could be produced because of the rapid evolution toward equal mass protostars. If the pro-

genitor cores have significant differential rotation, uniform-density and  $\rho \propto 1/r$  cores can easily produce the observed mass ratios, but it is still difficult to produce G-dwarf binaries with low mass ratios from cores with  $\rho \propto 1/r^2$ .

For close G-dwarf binary systems ( $a \gtrsim 5$  AU), the constraints are even more pronounced. Typically, we expect such binaries to accrete  $\approx 100$  times their ‘seed’ mass, yet the observed mass-ratio distribution is approximately flat (i.e. approximately 1/2 the binaries have  $q < 0.5$ ). It is effectively impossible for cores in solid-body rotation to produce such a mass ratio distribution if they are significantly centrally-condensed. Even for uniform-density cores, approximately 1/2 of the ‘seed’ binaries would need to have  $q < 0.1$ , although taking into account the effect of eccentricity (Section 5.3) it is probable that cores with nearly uniform-density profiles can reproduce the observations. If the cores have significant differential rotation, the observed mass ratios can be produced with cores that are as centrally-condensed as  $\rho \propto 1/r$ , but cores with  $\rho \propto 1/r^2$  are still excluded.

We note that, as discussed in Section 5, the results in Section 4 give the slowest possible evolution toward mass ratios of unity (unless the binary has a significant eccentricity). Thus, it may be even more difficult to form unequal mass binaries than suggested by the above discussion. Even taking the above numbers, with solid-body rotation the mass ratios of the ‘seed’ binaries must typically be  $q \approx 0.1 - 0.2$ . To obtain such mass ratios via direct fragmentation requires that the progenitor molecular cloud cores have significant asymmetries (e.g. Bonnell & Bastien 1992) which implies that they are formed and/or triggered to collapse by dynamical processes. Low mass ratios can also be obtained via rotational fragmentation (Section 1), but then the binary’s mass ratio will be driven toward unity even more rapidly. Thus, in reality, molecular cloud cores may have a degree of differential rotation.

In summary, **the observed mass-ratio distributions are most easily explained by cores that have density profiles that are less centrally condensed than  $\rho \propto 1/r$  (e.g. Gaussian), possibly with a small amount of differential rotation.** This is in good agreement with the observed density profiles of pre-stellar cores (Ward-Thompson et al. 1994; André, Ward-Thompson, Motte 1996; Ward-Thompson, Motte, & André 1999). If the progenitor cores rotate as solid-bodies it is essentially impossible to produce the observed mass-ratio distribution of close binaries if the cores are much more centrally condensed than a Gaussian-density profile. If differential rotation is allowed, cores with density profiles as steep as  $\rho \propto 1/r$  are feasible (with strong differential rotation), but cores with  $\rho \propto 1/r^2$  still cannot reproduce the observations.

### 6.2.2 Dependence of the mass ratio on the binary’s total mass

If all binary systems form by the same general process, regardless of a system’s final total mass (i.e. from the collapse of molecular cloud cores with the same properties, only more massive), and if the initial mass of a ‘seed’ binary (Section 6.1) is independent of the mass of the core (depending only on its initial separation), then **massive binaries should have more-equal mass ratios than low-mass binaries**

**of the same separation.** This is because systems with a larger final mass would have had to accrete more, relative to their initial mass, than systems with a lower final mass.

Unfortunately, unbiased surveys of stars more massive than G-dwarfs are only slowly becoming available. Preliminary results for O-star binaries (e.g. Manson et al. 1998) show a difference in the mass-ratio distribution between close ( $P \lesssim 40$  days;  $a \lesssim 1/2$  AU) and wide ( $P \gtrsim 10^4$  years;  $a \gtrsim 1000$  AU) systems, with close systems biased toward mass ratios of unity, but comparison between the mass-ratio distributions of high and low-mass binaries is not yet possible. In addition, Bonnell, Bate & Zinnecker (1998) recently proposed that O-stars form in a different way to lower mass stars, from the collision of less massive stars in very dense star-forming regions. This theory predicts a large frequency of close binaries for O-stars (due to tidal capture) with a mass-ratio distribution that is not determined by accretion from an infalling envelope. Thus, we strongly encourage surveys that will determine the mass-ratio distributions of B-, A-, and F-stars.

### 6.2.3 Formation of brown dwarf companions to solar-type stars

Given that it becomes more difficult to form binaries with low mass ratios as more gas is accreted by a binary, it is of interest to ask how easy it is to form stars with brown-dwarf companions (see also Bate 1998). Since wider binaries should have to accrete less gas, relative to their initial mass, to attain the same final total mass, then **the frequency of brown dwarf companions to solar-type stars should increase with separation.** Likewise, we expect that systems with lower final masses also accrete less relative to their initial masses so that **for the same range of separations, brown dwarf companions should be more frequent in systems with a lower total mass than in higher-mass systems.**

Taking the types of cores that most easily reproduce the mass-ratio distributions of low-mass stars (i.e. near-uniform density cores in solid-body rotation), we find that a brown dwarf companion to a solar-type star could be formed if an extreme mass ratio ( $q \approx 0.1$ ) was produced at fragmentation and the system subsequently increased its mass by a factor of  $\sim 20$  or less (Figure 9a). This implies that it may be quite easy to form brown dwarf companions to stars of around a solar mass or less with separations  $\gtrsim 10$  AU. Indeed, two wide systems have been found: GL 229B is a brown dwarf companion ( $0.02 - 0.06 M_{\odot}$ ) to a  $0.6 M_{\odot}$  M-dwarf with a separation of  $\approx 50$  AU (Nakajima et al. 1995); G 196-3B is a brown dwarf companion ( $0.02 - 0.04 M_{\odot}$ ) to a  $0.4 M_{\odot}$  M-dwarf with a separation of  $\approx 300$  AU (Rebolo et al. 1998).

However, close systems ( $\lesssim 10$  AU) need to accrete  $\approx 100$  times their initial mass in order to obtain a solar-mass primary and, due to the evolution of the mass ratio toward unity, it would be very difficult for the secondary to have the final mass of a brown dwarf after this amount of accretion. (Figure 9a). Therefore, **brown-dwarf companions to stars with masses  $\approx 1M_{\odot}$  and separations  $\lesssim 10$  AU are likely to be extremely rare or perhaps even nonexistent.** This prediction is supported by the recent radial-velocity searches for giant planets (see Marcy, Cochran & Mayor 1999 and references within). Although

many planetary candidates ( $M \sin i \lesssim 0.013 M_{\odot}$ ) have been found with separations less than a few AU, there are currently only 4 brown dwarf ( $0.013 M_{\odot} \lesssim M \sin i \lesssim 0.075 M_{\odot}$ ) candidates from  $\approx 600$  target stars and even these could be stellar companions with orbits nearly perpendicular to the line of sight (Marcy, Cochran & Mayor 1999).

Within this model, the easiest way to obtain such close systems with extreme mass ratios would be that they formed from cores with significant differential rotation, or that the companion was formed significantly *after* the primary. In the latter case, the primary would already have a significant fraction of its final mass and, hence, the protobinary would not have to increase its total mass by such a large factor. However, if this was achieved via the fragmentation of a circumstellar disc, then the fragmentation would have to occur after the primary and its disc had accreted a large fraction of the envelope, otherwise the secondary would still end up with a stellar mass due to subsequent accretion (Section 5.1 and Figure 14a).

### 6.3 Binary separations

In Section 4, we found that a binary's separation can evolve significantly due to accretion, increasing or decreasing by up to 2 orders of magnitude (Figures 9b to 14b). However, for most cases, if the binary's separation is increasing the PBE code also predicts that a massive circumbinary disc will be present. In test case 2 (Section 3.4; Figure 6), we found that if a massive circumbinary disc is present the interaction of the binary with the circumbinary disc is likely to negate the separation-increasing affect of the accretion and the separation will remain approximately constant.

Therefore, **we conclude that a binary's separation is likely to decrease or remain of the same order as its initial value during the accretion of the gaseous envelope.** After the accretion phase, if a binary has a circumbinary disc its separation is expected to decrease. Without a circumbinary disc, its separation is likely to increase as the circumstellar discs evolve viscously and transfer their angular momentum to the orbit of the binary. However, the angular momentum contained in the circumstellar discs is likely to be small compared to the orbital angular momentum of the binary and, therefore, the binary's separation is expected to increase by less than a factor of two.

### 6.4 Circumstellar discs

Bate & Bonnell (1997) studied the disc formation process in accreting protobinary systems and established criteria for the formation of circumstellar and circumbinary discs. They found that if a protobinary system only accretes gas with low specific angular momentum after its formation, the primary will have a circumstellar disc but the secondary may not. The reverse is not true; if a circumstellar disc is formed around the secondary, the primary will also have a disc. These conclusions can also be seen in the snapshots from the SPH test cases in Figures 4, 5, 7, and 8.

With the PBE code, we do not differentiate between gas that is directly accreted by a protostar and gas that is captured in its circumstellar disc (presumably to be accreted by the protostar at a later time). However, we do

determine the relative accretion rate on to the secondary and its circumstellar disc compared to the primary and its circumstellar disc  $\dot{M}_2/\dot{M}_1$  during formation of a binary (Figures 9d to 14d). We find that the relative accretion rate is  $\dot{M}_2/\dot{M}_1 \leq 1.3$  and in the majority of cases is less than unity. Therefore, **we expect that in most cases the circumsecondary disc will have a mass that is less than or similar to that of the circumprimary disc.** This conclusion is valid unless the circumprimary disc accretes on a shorter time-scale than the circumstellar disc. In fact, Armitage, Clarke & Tout (1999) showed that the circumsecondary disc is expected to accrete *more rapidly* than the circumprimary disc and, therefore, this effect should only be enhanced. This conclusion is in excellent agreement with the latest observations of circumstellar material around young binary systems. Ghez, White & Simon (1997) considered UV and NIR excess emission from the components of young binary systems and found that the excesses are either comparable or dominated by the primary, suggesting that the gas in circumstellar discs is either distributed similarly or preferentially around the primary.

The only cases where a circumsecondary disc may become significantly more massive than the circumprimary disc are those where the gaseous envelope has effectively been exhausted and accretion on to the circumstellar discs comes primarily from a circumbinary disc. In these cases, because the gas has very high angular momentum with respect to the binary, it will preferentially be captured by the secondary (Artymowicz & Lubow 1996; Bate & Bonnell 1997).

## 6.5 Circumbinary discs

From the results in Section 4, just as the mass ratio of an accreting protobinary evolves toward unity in the long-term, the more material that is accreted by a protobinary, the more likely it is that a circumbinary disc is formed. Therefore, following the same argument that we made for the mass ratios of binary stars, **we predict that closer binary systems are more likely to have circumbinary discs than wider systems with the same total mass.** Furthermore, if massive and low-mass binary systems via the same process, and if the initial mass of a ‘seed’ binary is independent of the mass of the core, then **massive binaries are more likely to have circumbinary discs than low-mass binaries of the same separation.**

The first of these predictions is in good agreement with recent observations. Jensen, Mathieu & Fuller (1996) surveyed 85 pre-main-sequence binary systems and found that, while emission presumably associated with circumbinary discs could be found around many close binaries (separations less than a few AU), circumbinary emission around binaries with separations of a few AU to  $\approx 100$  AU is almost entirely absent. The only exception was GG-Tau with a separation of  $\approx 40$  AU (Dutrey, Guilloteau & Simon 1994). Furthermore, Dutrey et al. (1996) performed an imaging survey of 18 multiple systems that could resolve circumbinary discs with radii  $\gtrsim 100$  AU and found only one circumbinary disc around UY-Aur which has a separation of  $\approx 120$  AU.

As with the mass-ratio evolution, the quantitative predictions depend on the properties of the progenitor cloud cores: **the more centrally-condensed a core is and/or the less differential rotation it has ( $\beta \leq 0$ ), the lower**

**the fraction by which a binary has to increase its mass before a circumbinary disc is formed.**

For cores in solid-body rotation, a uniform-density cloud leads to a significant circumbinary disc ( $M_{cb}/M_b > 0.05$ ) after a circular binary accretes  $\approx 2-40$  times its initial mass (depending on the initial mass ratio; Figure 9c). Using Figure 15, we would expect most *circular* binaries with separations  $a \lesssim 100$  AU to have circumbinary discs, while many with separations  $a \gtrsim 100$  AU should not have circumbinary discs. However, most wide binaries have large eccentricities (e.g. Duquennoy & Mayor 1991) and more material must be accreted by an eccentric binary before a circumbinary disc is formed (Section 5.3). Taking this into account, uniform-density cores in solid-body rotation are likely to produce circumbinary discs around most binaries with  $a \lesssim 10$  AU and some binaries with intermediate separations. However, very few should exist around binaries with separations  $a \gtrsim 100$  AU, in reasonable agreement with the observations.

For a core with  $\rho \propto 1/r$  (Figure 10), a binary can only increase its mass by a factor of  $\approx 1.5-6$  before a circumbinary disc is formed. In this case, most binaries with separations  $a \lesssim 100$  AU would be expected to have circumbinary discs, even taking eccentricity into account. With a  $1/r^2$ -density profile a binary can’t even double its mass before a circumbinary disc is formed (Figure 11) so that almost all binaries would be expected to have circumbinary discs, in strong disagreement with observations.

Differential rotation allows a binary to accrete more mass before a circumbinary disc is formed. In most cases, binaries formed from uniform-density cores (Figure 12) can accrete up to 100 times their initial mass without forming a massive circumbinary disc, meaning that even the closest binaries would not have circumbinary discs. Cores with  $1/r$ -density profiles (Figure 13) allow from 5 – 100 times a binary’s initial mass to be accreted so that most binaries with separations  $\lesssim 10$  AU and many with separations  $\lesssim 100$  AU would have circumbinary discs. Cores with  $1/r^2$ -density profiles would still produce discs around most binaries with separations  $a \lesssim 100$  AU.

Therefore, as with our predictions concerning binary mass-ratio distributions, **the circumbinary disc observations can be reasonably well explained if most binaries form from progenitor cores which are less centrally condensed than  $\rho \propto 1/r$  (e.g. Gaussian), possibly with a small amount of differential rotation.** Cores with  $\rho \propto 1/r$  are possible if there is significant differential rotation, but the singular isothermal sphere ( $\rho \propto 1/r^2$ ) cannot reproduce the observations even with extreme differential rotation.

## 7 CONCLUSIONS

We have considered a model for the formation of binary stellar systems which has been inspired by the results obtained from  $\approx 20$  years of study of the fragmentation collapsing molecular cloud cores. In the model, a ‘seed’ protobinary system forms, presumably via fragmentation, within a collapsing molecular cloud core and evolves to its final mass by accreting material from an infalling gaseous envelope.

We developed and tested a method which can rapidly follow the evolution of the mass ratios, separations and cir-

cumbinary disc properties of such binaries as they accrete to their final masses. Using this protobinary evolution code, we predict the properties of binary stars and how they depend on the pre-collapse conditions in their progenitor molecular cloud cores. These predictions and their comparison with current observations are discussed in detail in Section 6.

Briefly, we conclude that, if most binary stars form via the above model, binary systems with smaller separations or greater total masses should have mass ratios which are biased toward equal masses when compared to binaries with wider orbits or lower total masses. Similarly, the frequency of circumbinary discs should be greater for pre-main-sequence binaries with closer orbits or greater total masses. These conclusions can be understood because: binaries which are closer or have a greater final mass should accrete more gas relative to their initial masses than wider or lower-mass binaries; the specific angular momentum of the infalling gas relative to that of the binary is expected to increase as the accretion proceeds; and the accretion of gas with high specific angular momentum tends to equalise the mass ratio and forms a circumbinary disc. We also demonstrate that in a young binary which is accreting from an infalling gaseous envelope, the primary will generally have a circumstellar disc which is more massive or similar in mass to that of the secondary. All of these conclusions are in good agreement with the latest observations.

By making rough quantitative predictions of the properties of binary stars, we find that the observed properties of binary stars are most easily reproduced if the pre-collapse molecular cloud cores from which binaries form have radial density profiles between uniform and  $1/r$  (e.g. Gaussian) with near uniform rotation. This is in excellent agreement with the observed properties of pre-stellar cores (Ward-Thompson et al. 1994; André, Ward-Thompson, Motte 1996; Ward-Thompson, Motte, & André 1999). Conversely, the observed properties of binaries cannot be reproduced if the cores are in solid-body rotation and have initial density profiles which are strongly centrally condensed (between  $1/r$  and  $1/r^2$ ), and the singular isothermal sphere ( $\rho \propto 1/r^2$ ) cannot fit the observations even with strong differential rotation.

## ACKNOWLEDGMENTS

I am grateful to Ian Bonnell, Cathie Clarke and Jim Pringle for many helpful discussions and their critical reading of the manuscript.

## REFERENCES

André P., Ward-Thompson D., Motte F., 1996, *A&A*, 314, 625  
 Armitage P. J., Clarke C. J., Tout C. A., 1999, *MNRAS*, 304, 425  
 Artymowicz P., 1983, *Acta Astronomica*, 33, 223  
 Artymowicz P., Clarke C. J., Lubow S. H., Pringle J. E., 1991, *ApJ*, 370, L35  
 Artymowicz P., Lubow S. H., 1994, *ApJ*, 421, 651  
 Artymowicz P., Lubow S. H., 1996, *ApJ*, 467, L77  
 Balsara D., 1989, PhD thesis, Univ. of Illinois  
 Basu, S., 1997, *ApJ*, 485, 240  
 Bate M. R., 1995, PhD thesis, Univ. of Cambridge  
 Bate M. R., 1997, *MNRAS*, 285, 16

Bate M. R., 1998, in Rebolo R., Martin E. L., Zapatero Osorio M.R., eds., *Brown Dwarfs and Extrasolar Planets* (ASP Conf. Ser. 134). Brigham Young University, Provo, p. 273  
 Bate M. R., Bonnell I. A., 1997, *MNRAS*, 285, 33  
 Bate M. R., Bonnell I. A., Price N. M., 1995, *MNRAS*, 277, 362  
 Bate M. R., Burkert A., 1997, *MNRAS*, 288, 1060  
 Benz W., 1990, in Buchler J. R., ed., *The Numerical Modeling of Nonlinear Stellar Pulsations: Problems and Prospects*. Kluwer, Dordrecht, p. 269  
 Benz W., Bowers R. L., Cameron A. G. W., Press W., 1990, *ApJ*, 348, 647  
 Bonnell I. A., 1994, *MNRAS*, 269, 837  
 Bonnell I., Arcoragi J. -P., Martel H., Bastien P., 1992, *ApJ*, 400, 579  
 Bonnell I., Bastien P., 1992, *ApJ*, 401, 654  
 Bonnell I. A., Bate M. R., 1994a, *MNRAS*, 269, L45  
 Bonnell I. A., Bate M. R., 1994b, *MNRAS*, 271, 999  
 Bonnell I. A., Bate M. R., Zinnecker H., 1998, *MNRAS*, 298, 93  
 Bonnell I., Martel H., Bastien P., Arcoragi J. -P., Benz W., 1991, *ApJ*, 377, 553  
 Boss A. P., 1986, *ApJS*, 62, 519  
 Boss A. P., Bodenheimer P., 1979, *ApJ*, 234, 289  
 Burkert A., Bate, M.R., Bodenheimer P., 1997, *MNRAS*, 289, 497  
 Burkert A., Bodenheimer P., 1993, *MNRAS*, 264, 798  
 Burkert A., Bodenheimer P., 1996, *MNRAS*, 280, 1190  
 Burrows C. J., Stapelfeldt K. R., Watson A. M., Krist J. E., Ballester G. E., Clarke J. T., Crisp D., Gallagher J. S. III, Griffiths R. E., Hester J. J., Hoessel J. G., Holtzman J. A., Mould J. R., Scowen P. A., Trauger J. T., Westphal J. A., 1996, *ApJ*, 473, 437  
 Duquennoy A., Mayor M., 1991, *A&A*, 248, 485  
 Dutrey A., Guilloteau S., Simon M., 1994, *A&A*, 286, 149  
 Dutrey A., Guilloteau S., Duvert G., Prato L., Simon M., Schuster K., Menard F., 1996, *A&A*, 309, 493  
 Frank J., King A. R., Raine D. J., 1985, *Accretion Power in Astrophysics*. Cambridge University Press, Cambridge, p. 56  
 Ghez A. M., White, R. J., Simon M., 1997, *ApJ*, 490, 353  
 Halbwachs J. L., Mayor M., Udry S., 1998, in Rebolo R., Martin E. L., Zapatero Osorio M.R., eds., *Brown Dwarfs and Extrasolar Planets* (ASP Conf. Ser. 134). Brigham Young University, Provo, p. 308  
 Hall S. M., Clarke C. J., Pringle J. E., 1996, *MNRAS*, 278, 303  
 Hartmann L., Calvet N., Gullbring E., D'Alessio P., 1998, *ApJ*, 495, 385  
 Hernquist L., Katz N., 1989, *ApJS*, 70, 419  
 Jensen E. L. N., Mathieu R. D., Fuller G. A., 1996, *ApJ*, 458, 312  
 Kopal, Z., 1959, *Close Binary Systems* (International Astrophysics Series, Vol. 5). Chapman & Hall Ltd., London, p. 79-80  
 Lubow S. H., Artymowicz P., 1996, in Wijers R. A. M. J., Davies M. B., Tout C. A., eds., *Evolutionary Processes in Binary Stars*. Kluwer, Dordrecht, p. 53  
 Marcy G. W., Cochran W. D., Mayor M., 2000, in Mannings V., Boss A. P., Russell S. S., eds., *Protostars and Planets IV*. University of Arizona Press, Tucson, in press  
 Mason B. D., Gies D. R., Hartkopf W. I., Bagnuolo W. G. Jr., Brummelaer T. T., McAlister H. A., 1998, *AJ*, 115, 821  
 Mazeh T., Goldberg D., Duquennoy A., Mayor M., 1992, *ApJ*, 401, 265  
 Meglicki Z., Wickramasinghe D., Bicknell G. V., 1993, *MNRAS*, 264, 691  
 Monaghan J. J., 1992, *ARA&A*, 30, 543  
 Monaghan J. J., Gingold R. A., 1983, *J. Comput. Phys.*, 52, 374  
 Nakajima T., Oppenheimer B. R., Kulkarni S. R., Golimowski D. A., Matthews K., Durrance S. T., 1995, *Nature*, 378, 463  
 Nelson R., Papaloizou J. C., 1993, *MNRAS*, 265, 905  
 Norman M. L., Wilson J. R., 1978, *ApJ*, 224, 497  
 Pongracic H., 1988, PhD thesis, Monash Univ.

- Rebolo, R., Zapatero Osorio, M. R., Madrugá S., Bejar V. J. S.,  
Arribas S., Licandro J., 1998, *Science*, 282, 1309
- Stapelfeldt K. R., Krist J. E., Ménard F., Bouvier J., Padgett D.  
L., Burrows C. J., 1998, *ApJ*, 502, L65
- Steinmetz M., 1996, *MNRAS*, 278, 1005
- Tohline, J. E., 1982, *Fund. Cos. Phys.*, 8, 1
- Ward-Thompson D., Motte F., André P., 1999, *MNRAS*, 305, 143
- Ward-Thompson D., Scott P. F., Hills R. E., André P., 1994,  
*MNRAS*, 268, 276

This figure "fig04.gif" is available in "gif" format from:

<http://arxiv.org/ps/astro-ph/0002143v1>



This figure "fig05.gif" is available in "gif" format from:

<http://arxiv.org/ps/astro-ph/0002143v1>

This figure "fig07.gif" is available in "gif" format from:

<http://arxiv.org/ps/astro-ph/0002143v1>

This figure "fig08.gif" is available in "gif" format from:

<http://arxiv.org/ps/astro-ph/0002143v1>